

POROSITY AND ACTINIDE REDISTRIBUTION DURING
IRRADIATION OF (U,Pu)O₂*

W. J. Lackey, F. J. Homan, and A. R. Olsen

Metals and Ceramics Division, Oak Ridge National Laboratory
Oak Ridge, Tennessee 37830

NOTICE

This report was prepared as an account of work sponsored by the United States Government. Neither the United States nor the United States Atomic Energy Commission, nor any of their employees, nor any of their contractors, subcontractors, or their employees, makes any warranty, express or implied, or assumes any legal liability or responsibility for the accuracy, completeness or usefulness of any information, apparatus, product or process disclosed, or represents that its use would not infringe privately owned rights.

*Research sponsored by the U.S. Atomic Energy Commission under contract with the Union Carbide Corporation.

POROSITY AND ACTINIDE REDISTRIBUTION DURING
IRRADIATION OF (U,Pu)O₂

W. J. Lackey, F. J. Homan, and A. R. Olsen

ABSTRACT

Thermal-gradient-induced redistribution of porosity and fuel components during irradiation of (U,Pu)O₂ will alter the fuel thermal conductivity, melting point, mechanical properties, and radial heat generation profile sufficiently to influence fast breeder reactor fuel pin performance. Analytical models, which should prove useful in design and analysis of such fuel pins, were developed for predicting radial porosity and Pu:(U + Pu) profiles. The interrelated porosity and actinide redistribution models are kinetic and based on the evaporation-condensation mechanism of material transport. The models were shown to yield predictions in accord with experimentally measured porosity and actinide profiles for an irradiated pin containing stoichiometric fuel. The volume-averaged porosity of the columnar grain region of irradiated pins was 5.9 and $\geq 3.8\%$ after burnups of 0.7 and 4.2% FIMA, respectively. The columnar grains are thus more porous than previously believed.

INTRODUCTION

During irradiation of $(U,Pu)O_{2+x}$ fuel pins, large radial temperature gradients and smaller axial gradients result in a variety of chemical and electrical forces being exerted on the uranium, plutonium, and oxygen. These forces tend to cause component redistribution, which may occur via vapor phase transport, solid state diffusion, or a combination of the two mechanisms. Transport of material down the temperature gradient and migration of pores up the gradient alters the initially uniform distribution of porosity, uranium, plutonium, and oxygen in the fuel.

Our interest in the redistribution of porosity, the actinides, and oxygen is that such redistribution is likely to significantly influence the thermal and chemical behavior of fuel pins for liquid-metal-cooled fast breeder reactors (LMFBR) and gas-cooled fast breeder reactors (GCBR). As an example, the thermal conductivity of the fuel, and thus the fuel temperature profile in an operating fuel pin, is a function of the amount of porosity,^{1,2)} the plutonium-to-uranium ratio,^{3,4)} the oxygen content,⁵⁻¹⁰⁾ and other factors. The thermal conductivity of hypostoichiometric $(U,Pu)O_2$ fuel increases rapidly as the oxygen-to-metal ratio is increased and slightly as the uranium content increases. In addition, an increase in the plutonium-to-uranium ratio of the fuel adjacent to the central void will increase central fuel temperatures by altering the radial heat generation profile. Currently, a design criterion for the LMFBR and GCBR is that there be only a small probability that central fuel temperatures will reach the fuel melting point. Based on this criterion, thermal calculations by Sha, Huebotter, and Lo,¹¹⁾ which made allowance for the radial heat generation profile resulting from actinide redistribution,

show that the penalty in the maximum allowable linear heat rate may be as large as 2.5 kW/ft as a result of actinide redistribution. This is approximately 15% of the heat rate to melting and thus is a significant effect. The effect will be somewhat enhanced by the decrease in melting point arising from the higher plutonium content^{12,13)} and lower oxygen content¹³⁾ of the central fuel. However, the thermal conductivity of the fuel will be influenced simultaneously by the relocation of oxygen toward the cladding in a manner that will favorably influence the situation by reducing the central fuel temperature.

In this report we describe quantitative, computerized models that were developed for predicting the radial porosity and Pu:(U + Pu) profiles existing in (U,Pu)O₂ fuel pins during irradiation. The models are based on the evaporation-condensation mechanism and are time dependent. Both models have been incorporated into FMODEL^{14,15)} which is the ORNL-developed computer code for predicting fuel pin performance. Predictions are compared with experimentally measured porosity and Pu:(U + Pu) profiles for an irradiated (U,Pu)O₂ fuel pin. Since the porosity and actinide redistribution models are incorporated into a comprehensive fuels performance computer code, they can be used to determine the consequences of fuel component redistribution on the thermal and mechanical performance of (U,Pu)O₂ fuel pins.

REVIEW

Porosity Redistribution

Porosity initially present in the as-fabricated fuel, which is the type of porosity being considered, is generally believed to redistribute

by an evaporation-condensation mechanism.¹⁶⁻¹⁹⁾ The fuel vapor is transported along interconnected porosity or cracks or from the hot to cold side of closed pores, resulting in migration of porosity up the temperature gradient. Pores that remain smaller than about 1 μm migrate by surface or volume diffusion rather than by the evaporation-condensation mechanism.²⁰⁾ However, on a volume basis most of the fabrication porosity for pelletized²¹⁾ and certainly for Sphere-Pac or Vi-Pac fuels consists of the larger pores that migrate via the evaporation-condensation mechanism.

Although it is generally accepted that the hotter fuel densifies during irradiation under conditions that result in formation of columnar grains, the resulting radial porosity distribution is not adequately understood. Previous attempts^{22,23)} at measuring radial porosity distributions of irradiated fuel pins have not been particularly successful because of either appreciable scatter in the results, unavoidable confusion of fabrication porosity with fission-gas bubbles, or enhancement of the apparent void volume as a result of rounding of pore edges during metallographic polishing in a nonaqueous medium. Previous efforts^{1,24)} to incorporate in-reactor fuel densification into the thermal analysis generally have consisted of a step density approach, in which a different but constant porosity value is assigned to each of three zones with specified temperatures. The principal limitations to this approach are the uncertainty in the porosity assumed for each zone and the inability of this approach to consider the kinetic aspect of restructuring.

Time dependence of the restructuring process is important when modeling fuel-cladding mechanical interactions, which result from differential thermal expansion between the fuel and cladding during startup

or during overpowering of the fuel pin. Restructuring reduces fuel temperatures and consequently thermal expansion; but without knowing the rate of restructuring, it is not possible to determine maximum fuel temperatures or the rate of decrease of the mechanical interaction with decreasing fuel temperatures. To calculate radial porosity distributions, Rim and Fenech²⁵⁾ have analytically modeled pore migration in a manner similar to that described in this report. Details of their calculations, which resulted in high densities (> 99% of theoretical) for the columnar grain region after short irradiation times, were not reported.

Actinide Redistribution

Concurrent with material transport, preferential transport of uranium or plutonium would establish gradients in the plutonium-to-uranium ratio, and such gradients^{19, 26-30)} have been observed along radii of irradiated (U,Pu)O₂ fuel pins. Actinide redistribution has also been observed³¹⁻³⁵⁾ in out-of-reactor (U,Pu)O₂ thermal gradient tests. In fuel pins containing hyperstoichiometric, stoichiometric, or slightly hypostoichiometric (U,Pu)O₂ that experience columnar grain growth, the postirradiation plutonium-to-uranium ratio typically increases with temperature (e.g., on approaching the central void). Concentration of plutonium into molten fuel can produce gradients in the actinide content,^{12, 13, 33, 36, 37)} and this mechanism will likely dominate in center-melted fuels. However, fuels that experience center melting are not treated further in this paper.

The gradient in actinide composition could be the result of:

1. enrichment of the hotter fuel in plutonium as a result of formation of a uranium-rich vapor over the hotter fuel, migration of the vapor

down the partial pressure gradient, and condensation at some lower temperature;^{38,39)} or

2. preferential solid-state thermal diffusion^{31,38)} of plutonium or uranium along the temperature gradient as a result of a thermally induced cation vacancy gradient or electrical potential gradient.

The only previous attempt to develop a vapor-phase transport model for quantitatively predicting radial Pu:(U + Pu) profiles is that of Aitken and Evans.^{40,41)} They calculated vapor-phase compositions according to the method of Rand and Markin and used these values to calculate solid compositions based on the assumption (which at the time appeared to be reasonable) that the Pu:(U + Pu) ratio in the vapor phase was constant throughout the fuel pin. It has since been shown^{42,43)} that this approach yields erroneous results.

Although the idea that differences in the partial pressures of uranium- and plutonium-bearing vapor could possibly result in preferential transport and therefore separation of the actinides is not new,^{38,39)} several previous investigators^{28,31)} concluded that actinide redistribution occurred primarily by the solid state diffusion mechanism. Although the evidence is not infallible, we^{19,42)} and others^{33-35,43)} have recently concluded that redistribution via the vapor phase is the most likely mechanism. Experimental evidence that a vapor phase mechanism is operative, at least for stoichiometric fuel, is presented later in this report.

The most important previous thermodynamic calculation of vapor phase actinide redistribution is that of Rand and Markin.³⁹⁾ Although they stopped short of developing a quantitative model for predicting

radial Pu:(U + Pu) profiles in the solid fuel, they compiled the necessary thermodynamic data and calculated the vapor-phase composition existing in equilibrium over solid $(U,Pu)O_{2\pm x}$ at temperatures up to 2000°K. Their calculations showed that for hyperstoichiometric mixed oxide the vapor phase was rich in uranium compared to the solid, and consequently they predicted that the Pu:(U + Pu) ratio of the hotter solid fuel would increase during irradiation. On the other hand, for appreciably hypostoichiometric oxides, their calculations indicated that the vapor over the hotter fuel would be rich in plutonium compared to the solid composition, and thus the Pu:(U + Pu) ratio of the hotter fuel would decrease. For $U_{0.85}Pu_{0.15}O_{2-x}$ at 2000°K their calculations showed the critical oxygen-to-metal ratio, that is, the stoichiometry at which the Pu:(U + Pu) ratio of the vapor equaled that of the solid, to be 1.978. However, this is not a unique point in terms of the initial or overall oxygen-to-metal ratio of the unirradiated fuel since, as will be shown later, the Pu:(U + Pu) ratio of the vapor phase is strongly dependent on the fuel temperature as well as the extent to which the oxygen-to-metal ratio of the hotter fuel is changed as a result of oxygen redistribution.

There is conflicting experimental evidence for comparison to Rand and Markin's predictions of the oxygen-to-metal ratio and the temperature where the vapor phase becomes rich in plutonium under isothermal conditions. Oshe and Olson's⁴⁴⁾ measurements of the vapor phase composition over $U_{0.85}Pu_{0.15}O_{2-x}$ are in general agreement with the calculations of Rand and Markin,³⁹⁾ while Battles et al.⁴⁵⁾ observed the

vapor over $U_{0.8}Pu_{0.2}O_{2-x}$ at 2241°K to be uranium rich even at oxygen-to-metal ratios as low as about 1.93.*

Neither irradiation tests nor out-of-reactor thermal gradient tests clarify the influence of stoichiometry on controlling whether the vapor phase will be rich in uranium or plutonium. Excluding molten fuel tests, no irradiation test to date has resulted in a decrease in the Pu:(U + Pu) ratio in the vicinity of the central void; however, only one fuel pin has been examined for which the oxygen-to-metal ratio was less than 1.98. In this test,⁴⁶⁾ in which the oxygen-to-metal ratio was 1.95, the Pu:(U + Pu) ratio at the central void increased from 20 to 21% rather than decreasing. For this test neither the linear heat rate nor whether or not the pin operated with molten fuel were reported. There have been only three out-of-reactor thermal gradient tests with oxide of low oxygen-to-metal ratio. These tests, as well as the irradiation test just described, are summarized in Table 1. Contrary to what one would have predicted, based on the vapor composition determinations of Oshe and Olson⁴⁴⁾ and the calculations of Rand and Markin,³⁹⁾ an increase in the Pu:(U + Pu) ratio of the hotter fuel was observed for the tests where the oxygen-to-metal ratios were 1.93 and 1.95. For the fuel with an oxygen-to-metal ratio of 1.96, no segregation was detected by alpha

*The different plutonia contents of the solids used by Oshe and Olson and Battles et al. perhaps account for the observed difference in vapor phase composition. However, Battles et al. have suggested that the tungsten effusion cells used by Oshe and Olson might have reacted with the oxide and thus introduced errors in the measurements. On the other hand, the calibration used by Battles et al. appears inferior to that of Oshe and Olson.

autoradiography,* indicating that the Pu:(U + Pu) ratio of the solid and vapor was similar. The results for this specimen at first appear to contradict the findings for the specimens with lower oxygen-to-metal ratios. That is, since the vapor and solid phases were similar in plutonium content for the specimen with an oxygen-to-metal ratio of 1.96, one would expect the vapor over the two specimens with lower oxygen-to-metal ratios to be rich in plutonium. This would have resulted in a decrease rather than the observed increase in plutonium content of the hotter fuel. It is possible that the longer heating time for the two specimens of lowest oxygen-to-metal ratio allowed another mechanism of segregation (solid-state diffusion) to predominate. This suggestion is discussed further in the following paragraph. Beber et al.³⁴⁾ have demonstrated in an out-of-reactor thermal gradient test that the vapor phase emanating from hypostoichiometric (U,Pu)O₂ can have a Pu:(U + Pu) ratio as large as 0.25. Vapor of that composition was deposited near the end of the heating period when the hotter solid had a Pu:(U + Pu) ratio of about 0.24 and an unknown but likely low oxygen-to-metal ratio. We,⁴²⁾ as well as others,⁴³⁾ have reached the conclusion that until more experimental measurements are conducted the most reliable values for the vapor phase composition are those calculated according to the method of Rand and Markin.³⁹⁾

A plausible explanation for all of the apparent contradictions of previous workers, except the apparent differences in the mass spectrometric measurements of Oshe and Olson⁴⁴⁾ and Battles et al.,⁴⁵⁾ is that

*Our work with alpha autoradiographs obtained with cellulose nitrate film shows the sensitivity to be about 20% of the plutonium content. For example, a change in the Pu:(U + Pu) from 0.20 to 0.16 is just detectable.

the vapor over markedly hypostoichiometric oxide is plutonium rich compared to the solid, in agreement with Rand and Markin; but solid-state thermal diffusion (Soret effect) of plutonium up the temperature gradient is the dominant transport mechanism for markedly hypostoichiometric oxide except for short irradiation times. Previously we stated that vapor phase transport was the most likely mechanism for actinide redistribution; however, all the evidence upon which this conclusion was based was derived from stoichiometric material. For appreciably hypostoichiometric oxide the Soret effect possibly dominates for longer irradiation times. Other investigators³¹⁻³⁴) have compared experimentally measured Pu:(U + Pu) profiles with predictions based on actinide redistribution via the Soret effect. Unfortunately, estimates of the heat of transport Q_A^* have varied considerably from experiment to experiment, and more comparisons of observed and calculated profiles are needed before definitive calculations of the Soret effect can be performed. In this regard, it is interesting to note that all the out-of-reactor thermal gradient tests have involved *axial* gradients. Irradiation tests and out-of-reactor *radial* gradient tests employing fuel of different initial oxygen-to-metal ratios and densities would be of considerable value in establishing the relative importance of vapor phase and solid-state transport. Radial gradients are preferred over axial gradients because of significant errors³⁴) associated with free evaporation of material from the hot end of an axial specimen and condensation in the void between the specimen and the container. Axial gradient tests do not satisfactorily simulate irradiation of fuel pins because in axial gradient tests there is no fuel material between the hotter end of the specimen and cooler portions of the container so free evaporation can occur.

Oxygen Redistribution

Although this paper deals primarily with the porosity and actinide profiles present during irradiation, it is also necessary to consider oxygen redistribution since porosity and actinide redistribution depend on fuel stoichiometry. Also, oxygen redistribution is important since the thermal conductivity of the fuel, and therefore fuel temperatures, depends on the oxygen-to-metal ratio. Although the present understanding of thermal-gradient-induced oxygen redistribution is far from complete, several investigators have observed oxygen gradients in irradiated $(U,Pu)O_2$ ^{1,47,48)} as well as in out-of-reactor $(U,Pu)O_2$ thermal gradient tests.^{40,49-51)} Excluding tests in which a portion of the fuel was molten, there has not been a single irradiation test in which the oxygen profile has been adequately measured. This results from the fact that the measurements are extremely difficult for small pins plus the unfortunate but frequent choice of center-melted pins for use in such studies. Oxygen profiles have been adequately measured in out-of-reactor thermal gradient tests, but such work suffers from the fact that all such tests employed axial rather than radial gradients. Aitken et al.^{40,50,52)} have reviewed the available data and discussed possible mechanisms for oxygen redistribution. Briefly, for hyperstoichiometric fuel oxygen migrates toward the hotter fuel, while for hypostoichiometric mixed oxide oxygen migrates toward the cooler fuel. In principle, the steady-state oxygen profile could be the result of: (1) cyclic vapor-phase transport of CO_2 and CO or H_2O and H_2 ; (2) solid-state oxygen diffusion (Soret effect for oxygen redistribution — not to be confused with the Soret effect for actinide redistribution); or (3) a combination of vapor-phase and

solid-state transport mechanisms. For hyperstoichiometric oxide the H_2O and CO_2 pressures are large enough that vapor-phase transport is most likely and the oxygen-to-metal profile is calculated from the assumption that the $H_2O:H_2$ or $CO_2:CO$ ratio is constant throughout the fuel pin, as first proposed by Rand and Roberts⁵³⁾ and elaborated on by Rand and Markin.³⁹⁾ For hypostoichiometric mixed oxide the vapor pressures are significantly lower, making transport via the vapor phase sluggish, and therefore solid-state diffusion of oxygen probably predominates. Analysis by Aitken et al.^{50, 52)} for hypostoichiometric oxide indicated that the assumption of a constant $H_2O:H_2$ or $CO_2:CO$ ratio leads to overpredicting the extent of oxygen redistribution. They therefore chose to explain experimentally observed oxygen profiles for hypostoichiometric oxide on the basis of solid-state diffusion of oxygen and employed an irreversible thermodynamic approach in which the value of the heat of transport applicable to oxygen redistribution depended on the stoichiometry. This approach is described in detail later in that it was selected for use in our models since it appears most appropriate for the range of stoichiometry of interest. However, the available data for relating the heat of transport to stoichiometry are limited and additional experimental work is needed.

THIS WORK

The analytical models that we have developed for porosity and actinide redistribution are based on the evaporation-condensation mode of material transport. The available physical evidence indicates that this is the predominant mode of material movement, at least during the

early stages of irradiation when the major changes in as-fabricated fuel structure and actinide distribution are occurring.

Evidence of Vapor-Phase Transport

Our reasons for believing that fuel restructuring and, at least for stoichiometric or slightly hypostoichiometric oxide, actinide redistribution occur by vapor transport are best explained by reference to Figs. 1 and 2. Figure 1 shows the region of transition from columnar to equiaxed grains for a low burnup $U_{0.85}Pu_{0.15}O_{2.00}$ fuel pin (43-112-3). This fuel pin consisted of coarse and fine fractions of microspheres clad in a 0.252-in.-OD stainless steel tube having a 0.010-in. wall. The fuel length was 3 in., and the initial smear density was 81.4% of theoretical. The pin was irradiated in the Engineering Test Reactor (ETR) with a cladding inner surface temperature of 320°C, and the linear heat rate and burnup at the position examined were 13.6 kW/ft and 0.7% FIMA, respectively. It is apparent that fuel vapor was deposited in the form of dendrites onto the hot side of microspheres. Electron microprobe analysis showed the deposited fuel to be rich in uranium compared to both the microspheres and the adjacent columnar grains. The approximate Pu:(U + Pu) ratio of the deposited fuel was 0.12; the deposits may have a Pu:(U + Pu) ratio as low as 0.08.

Additional evidence that uranium is preferentially transported, at least for stoichiometric fuel, is obtained by comparison of the photomicrograph and alpha autoradiograph (Fig. 2) of a similar $U_{0.85}Pu_{0.15}O_{2.00}$ pin (43-115-4) irradiated in the ETR to a burnup of 4.2% FIMA at a

time-averaged linear heat rate of 13.4 kW/ft (initially the heat rate was 14.7 kW/ft, but as a result of burnup it decreased to a final value of 11.8 kW/ft). The alpha autoradiograph shows the typical increase in plutonium activity near the central void. What is unique are the spherical "islands" of average plutonium content in the cooler regions of the columnar grain structure. These islands are the remnants of the original coarse microspheres. Since the dense oxide surrounding the islands is low in plutonium content, we believe this is strong evidence for vapor transport of uranium-rich fuel radially down the temperature gradient.

Having evidence for vapor-phase fuel transport, we have developed a mathematical model to calculate the extent of restructuring, porosity distributions, and actinide distributions as a function of the fuel pin fabrication and irradiation conditions. For clarity, the description of this model is divided into three parts: one dealing with oxygen redistribution, another with porosity movement, and the third with actinide redistribution. Oxygen redistribution is described first, since both porosity and actinide redistribution are dependent on the oxygen profile.

Oxygen Redistribution Model

The first step in the analytical procedure consists of calculating the radial temperature profile from thermal conductivity values applicable to the initial porosity of the fuel. For this purpose, the fuel in an axial segment of the fuel pin is divided into 30 radial increments of equal volume. Next, the temperature profile and the initial (i.e., overall) oxygen-to-metal ratio are used to calculate the oxygen-to-metal

radial distribution according to the previously mentioned irreversible thermodynamic approach. Equation (1) is the basic equation involved in calculating the oxygen distribution.

$$\frac{x_2}{x_1} = \exp \left[\frac{Q_0^*}{R} \left(\frac{1}{T_2} - \frac{1}{T_1} \right) \right], \quad (1)$$

where

Q_0^* = heat of transport for oxygen,

x = deviation from stoichiometry ($MO_{2\pm x}$),

T_1, x_1 = absolute temperature and deviation from stoichiometry at the cold node of the volume increment,

T_2, x_2 = temperature and deviation from stoichiometry at the hot node of the volume increment, and

R = gas constant.

An additional feature of the oxygen redistribution model, which was deemed necessary from the experimental work of Evans et al.,⁴⁹⁾ is that the oxygen-to-plutonium ratio is not allowed to go below a value of 1.575. For fuel containing 20% Pu, this corresponds to limiting the oxygen-to-metal ratio to values above 1.915. Evans et al.⁴⁹⁾ also showed that the value of Q_0^* depends on the oxygen-to-metal ratio.

We generated Eq. (2) from their data to describe this dependence. The equation gives the value of Q_0^* in kilocalories.

$$\begin{aligned} \ln(-Q_0^*) = & 25285297.41 - 51549175.60 (O/M) + 39409641.35 (O/M)^2 \\ & - 13390495.52 (O/M)^3 + 1706153.647 (O/M)^4 \quad . \quad (2) \end{aligned}$$

The equation is valid for oxygen-to-metal ratios, O/M, between 1.94 and 1.996. Below O/M = 1.94, we recommend $Q_0^* = -7.1$ kcal. For an O/M = 2.000, we assume that no redistribution of oxygen occurs.

To calculate the oxygen profile, Eq. (1) is applied in succession to each of the 30 radial fuel increments, beginning with the outermost increment. First a value is assumed for the oxygen-to-metal ratio of the fuel adjacent to the cladding, and then with Eq. (1) the oxygen-to-metal ratio of the fuel at the inner node of this outermost fuel increment is calculated. This value is then used with Eq. (1) to calculate the oxygen-to-metal ratio at the next innermost node. In this manner the oxygen-to-metal ratio is calculated for each of the nodes. These values are then used to calculate the volume-averaged oxygen-to-metal ratio. In general, the value calculated for the volume-averaged oxygen-to-metal ratio will not be in agreement with the initial, or overall, fuel stoichiometry, and a new value must be assumed for the stoichiometry of the fuel adjacent to the cladding. The calculations are repeated until the calculated volume-averaged oxygen-to-metal ratio is in agreement with the initial, or overall, oxygen-to-metal ratio of the fuel pin. Since the temperature profile changes as restructuring occurs, the calculations must be repeated for a series of time steps spanning the irradiation time. In addition, the overall oxygen-to-metal ratio is adjusted for the effect of burnup by increasing the ratio by 0.006 for each percent FIMA.³⁹⁾ To account for the buffering action afforded by oxidation of molybdenum, the oxygen-to-metal ratio is not increased beyond the stoichiometric composition.

Since the thermal conductivity of (U,Pu)O₂ depends strongly on the oxygen-to-metal ratio as well as temperature and porosity, the thermal conductivity values used in the thermal analysis are calculated at each node from Eq. (3):

$$k = 0.01524 + \frac{1}{(0.9702 - 0.4465D)T} + 0.5841 \times 10^{-12} T^3 + \frac{360.2}{(2.04 - O/M)T^2}, \quad (3)$$

where

k = thermal conductivity (W cm⁻¹ °C⁻¹),

T = temperature, °C,

D = fractional density, and

O/M = stoichiometry.

Equation (3) was recently developed by Laskiewicz et al.¹⁰⁾ It is based on a very limited amount of data, and additional experimental work, particularly above 1400°C, is urgently needed. The equation overpredicts the conductivity at the higher temperatures, and we have chosen to use the value calculated for 2200°C for all higher temperatures.

Porosity Redistribution Model

The porosity redistribution model is based on the equation for the velocity of migration of a pore moving by the evaporation-condensation mechanism. The velocity equation, as proposed by de Halas and Horn¹⁷⁾ and modified by Nichols,¹⁸⁾ is:

$$v = \frac{Kp_0 \exp(-H/RT)}{PT^{3/2}} \frac{dT}{dx}, \quad (4)$$

where

$K =$ a material constant $= 3.364$,

$p_0 =$ a material constant,

$H =$ heat of vaporization,

$T =$ temperature, °K,

$\frac{dT}{dx} =$ temperature gradient, °K/cm, and

$P =$ total pressure in pore, atm.

It is to be noted that $p_0 \exp(-H/RT)$ is the sum of the partial pressures of the uranium- and plutonium-bearing vapor species. Normally, constant values are assigned to p_0 and Q for the purpose of calculating the vapor pressure of the fuel. However, to allow for the reduction in vapor pressure that accompanies decreases in the oxygen-to-metal ratio of $(U,Pu)O_2$ we have modified Eq. (4) by replacing $p_0 \exp(-H/RT)$ with Eq. (5), which gives the actinide vapor pressure in atmospheres over $U_{0.8}Pu_{0.2}O_{2-x}$ as a function of oxygen-to-metal ratio and the Kelvin temperature.

$$\ln p_0 \exp(-H/RT) = -212.275 + 65.842 (O/M) + 8.9453 \times 10^{-2} T - 2.55399 \\ \times 10^{-2} (O/M) T + 2.9560 (O/M)^2 - 5.6541 \times 10^{-6} T^2 \quad (5)$$

Equation (5) was obtained by least-squares analysis of actinide vapor pressures calculated with equilibrium thermodynamics as described in Appendix A. Such vapor pressure calculations (also, see Appendix B) revealed that for the same vapor pressure the temperature of $U_{0.8}Pu_{0.2}O_{1.94}$ must be about 100°C higher than that of the stoichiometric oxide. Thus, the calculations and recent experimental measurements¹⁰⁾ indicate that the extent of restructuring depends sufficiently on the oxygen-to-metal ratio to warrant the inclusion of Eq. (5).

The pore velocity as given by Eq. (4) is independent of pore size and shape. Therefore, according to this model, all pores at a given radius within the fuel move with the same velocity. It is not obvious what the total pressure, P , within the pores should be. Two possibilities were considered. One approach is to assume that the pores are open to the gas plenum and the pressure in the pores is the same as the plenum pressure. A second assumption is that the porosity in regions of density less than 90% of theoretical are open to the gas plenum, but regions of greater density have closed pores. The pressure in the closed pores would then be related to the temperature of the region and the pressure that existed in the pores when they closed. For the fuel pin discussed in the following section, the calculated porosity distribution did not significantly depend on which of the above assumptions were employed. We believe, however, the latter assumption is more realistic.

To calculate the time-dependent change in the porosity distribution in an operating fuel pin, consider the physical situation associated with one radial increment of an axial segment of unit length. The increment is bounded by R_i and R_{i+1} (the inner and outer radii, respectively) and characterized by temperatures T_i and T_{i+1} , and temperature gradients $(dT/dx)_i$ and $(dT/dx)_{i+1}$. The pore velocities at R_i and R_{i+1} are v_i and v_{i+1} , respectively. Assume that the axial fuel segment under consideration initially contains N pores, each with volume V . The number of pores in the i th radial increment is then given by

$$N_i = A_i N / A_T, \quad (6)$$

where

A_i = cross-sectional area of the i th radial increment, and

A_T = cross-sectional area of the entire fuel segment.

In t seconds all pores in the annulus bounded by R_i and $R_i + v_i t$ will leave the i th radial increment, and all pores in the annulus bounded by R_{i+1} and $R_{i+1} + v_{i+1} t$ will enter the increment. The number of pores leaving will therefore be

$$N'_i = \frac{N_i \pi}{A_i} \left[(R_i + v_i t)^2 - R_i^2 \right], \quad (7)$$

and the number of pores entering the increment will be

$$N'_{i+1} = \frac{N_{i+1} \pi}{A_{i+1}} \left[(R_{i+1} + v_{i+1} t)^2 - R_{i+1}^2 \right]. \quad (8)$$

Thus, the i th increment has gained $N'_{i+1} - N'_i$ pores. The total number of pores now in the increment is

$$N''_i = N_i + N'_{i+1} - N'_i. \quad (9)$$

The fractional porosity in the i th increment is now

$$P_i = N''_i(V)/A_i, \quad (10)$$

whereas the initial porosity fraction was

$$(P_i)_0 = NV/A_T. \quad (11)$$

The ratio

$$P_i/(P_i)_0 = A_T/A_i (N''_i/N) \quad (12)$$

can be expressed as in Eq. (13) by making use of Eqs. (6) through (9) and the fact that the ratio N_{i+1}/N_i equals $(P_{i+1})_0/(P_i)_0$ (i.e., the ratio of porosity in the $i + 1$ th and i th increments at the beginning of the time period):

$$\frac{P_i}{(P_i)_0} = 1 + \frac{\pi (P_{i+1})_0}{A_{i+1} (P_i)_0} [(R_{i+1} + v_{i+1}t)^2 - R_{i+1}^2] - \frac{\pi}{A_i} [(R_i + v_i t)^2 - R_i^2] \quad (13)$$

Note that the initial number of pores, N , and volume of a single pore, V , have cancelled out of the expression. Equation (13) gives the desired quantity P_i , the porosity of the i th radial increment at the end of the time period.

This approach depends on the assumption that the pore velocity v_i is described by the temperature T_i and temperature gradient $(dT/dx)_i$ not just at the radial node R_i but throughout the entire neighborhood of this node. This is only approximately correct. In the FMDEL code,^{14,15} temperature and temperature gradients are calculated only at radial nodes and assumed to vary linearly between nodes. To prevent large errors from being introduced into the porosity calculations, the time step t is restricted so that the distance $v_i t$ can never exceed $(R_{i+1} - R_i)/3$. Temperature distributions are recalculated after every period of t seconds, and the new temperatures and temperature gradients are used in the subsequent porosity distribution calculation. This sequence is repeated until the entire time period of interest has been considered.

The temperature gradients in a cylindrical fuel pin are quite high in the fuel region adjacent to the cladding and diminish to zero as the

thermal center is approached. Strict application of Eq. (4) would result in the pore velocity going to zero as the pores approach the thermal center and subsequent pileup of pores in the inner radial increment. We have thus approximated the temperature gradient in the vicinity of the inner radial node by setting it equal to the gradient at the second node.

Comparison of Measured and Predicted Porosity Distributions

The amount of porosity that existed at various known radii was measured for an irradiated $U_{0.85}Pu_{0.15}O_{2.00}$ fuel pin (43-112-3) that operated long enough (28 effective full-power days) for appreciable restructuring to occur but not long enough for significant fuel swelling. The fuel pin consisted of coarse and fine fractions of microspheres clad in a 0.252-in.-OD stainless steel tube having a 0.010-in. wall. The fuel length was 3 in., and the initial smear density was 81.4% of theoretical. The pin was irradiated in the ETR, and the linear heat rate and burnup at the position examined were 13.6 kW/ft and 0.7% FIMA, respectively. The amount of porosity present was determined with a Quantimet* image analyzing computer using 500 \times light micrographs taken along three radii of an unetched, aqueous¹ polished transverse section. Electron microscopy⁵⁴⁾ of the restructured fuel showed that the amount of porosity that was not resolvable at 500 \times to be negligible. As a check on the Quantimet, the amount of porosity apparent in several of the micrographs was determined by manual point counting using a grid consisting of 30 lines per inch.

*Quantimet Model B, Image Analyzing Computers, 40 Robert Pitt Drive, Monsey, New York.

A composite photomicrograph of a portion of the cross section examined is shown in Fig. 3(a). Also shown in Fig. 3 is a plot of porosity versus fractional fuel radius. The points shown are the measured values, and the distribution calculated with the model is given by the solid curve. The measured and predicted porosities are in very good agreement. Also, the good agreement between the Quantimet and manually determined porosities gives confidence in the experimental measurements. The increased scatter of the experimentally determined porosity values nearest the central void is the result of actual variations in the fuel porosity adjacent to the central void rather than measurement error.

The predicted size of the central void was larger than the observed size, perhaps as a result of uncertainty in the initial smear density at the cross section examined or as a result of axial transport of fuel by evaporation-condensation. Axial transport resulting in only a 3% increase in the amount of fuel present at the section examined would alone account for the discrepancy. There was no direct evidence that axial transport did or did not occur.

Both light and electron microscopy revealed that only a very negligible amount of material was transported beyond a fractional fuel radius of 0.68. Further, the cooler fuel did not appear to have sintered sufficiently to produce a gap at the fuel-cladding interface. Therefore, the total quantity of porosity in the region between fractional fuel radii of 0.68 and 1.0 was assumed to be the same as the preirradiation value of 18.6%. This assumption is in accord with the model since restructuring was not predicted for this region.

These measurements show the columnar grain region to be, on the average, considerably more porous than corresponds to the previously generally assumed density values of 97 (ref. 24) to 99% (ref. 1) of theoretical. We believe the higher porosity observed here (a volume-averaged value of 5.9% for the columnar grain region) is typical for pins with smear densities in the range of 80 to 85% of theoretical, since pins irradiated to about 5% FIMA in both a thermal and fast flux show similarly high porosities for the columnar grain regions. As an example, Fig. 4 shows the microstructure and measured radial porosity distribution of the previously described $U_{0.85}Pu_{0.15}O_{2.00}$ fuel pin (43-115-4) from the medium-burnup thermal flux test. Contrary to the case for the previously described low-burnup pin, the volume occupied by fission-gas bubbles that are too small to be resolved at 500 \times is probably not negligible. Consequently, the porosity data in Fig. 4 should be regarded as minimum values. Even so, the measured volume-averaged porosity for the columnar grain region was 3.8%, which is larger than previously assumed values. Visual comparison of the micrograph of this pin with that shown in Fig. 5 of a pin irradiated in EBR-II shows that similarly high porosities occur in pins irradiated in a fast neutron flux.

An interesting feature of the latter two fuel pins is that at fractional fuel radii of about 0.9 there is no evidence of deposited fuel, and the porosity is apparently similar to that of the as-fabricated pin. However, immediately adjacent to the cladding, fuel has been vapor deposited. Electron microprobe analysis showed the deposits to be principally mixed oxide. The low-burnup pin contained only an insignificant amount of such deposited fuel. Deposition of fuel on the cladding inner

surface, which is indicated by the dashed lines in Fig. 4, undoubtedly leads to a gradual increase in the gap conductance as the irradiation progresses.

Sensitivity of Fuel Temperatures to Porosity Distribution

To determine the sensitivity of fuel temperatures to the radial porosity distribution, temperatures were calculated for the low-burnup fuel pin (43-112-3) discussed previously for two cases. The calculations were based on: (1) our best estimate of the porosity before the experimental measurements, and (2) the experimentally measured porosity distribution. For the first case, the porosity distribution was approximated by assuming that the fuel restructures to a density of 97% of theoretical where the temperature exceeds 1750°C to a density of 92% between 1450 and 1750°C, and not at all below 1450°C. In the second case, the experimentally measured porosity distribution was used in the temperature calculations. The porosity profiles and calculated temperatures are plotted in Fig. 6. For the high-temperature region the temperatures calculated from the experimentally measured porosity distribution are about 200°C higher. This demonstrates the need for accurate knowledge of the porosity distribution if one wishes to operate fuel pins at the maximum linear heat rate possible without experiencing fuel melting.

Actinide Redistribution Model

The actinide redistribution model is based on the combined calculation of the amount of fuel added or removed from each of a series of radial increments plus calculation of the Pu:(U + Pu) ratio of the vapor-transported material. That is, since the initial Pu:(U + Pu) ratio of

each radial increment is known and the amount of fuel transported into and out of each increment is calculated with the previously described model for porosity redistribution, the Pu:(U + Pu) ratio of each increment at the end of the time step can be calculated if the composition of the vapor-transported material is known. The composition of the material transported from one radial increment to another is calculated on the bases of the equilibrium thermodynamic data compiled by Rand and Markin³⁹⁾ as described in Appendix A. The unique feature of the model is that it combines the porosity redistribution model with calculated vapor compositions to yield the resulting Pu:(U + Pu) radial profile for a fuel pin. The model should apply for predicting actinide redistribution that occurs by evaporation-condensation regardless of whether the vapor is transported across a closed pore or along cracks or interconnected porosity. This is reasonable because the Pu:(U + Pu) content of the vapor would equilibrate with the solid it contacts on moving down the temperature gradient, independent of the geometrical configuration.

The oxygen-to-metal distribution is needed at each node to calculate the Pu:(U + Pu) ratio of the vapor phase since the composition of the vapor is sensitive to the oxygen potential as well as temperature and the Pu:(U + Pu) ratio of the solid. The calculations for a given time step are completed by calculating the Pu:(U + Pu) ratio of each increment based on the quantity and composition of material transported into and out of the increment. The necessary equations were derived as follows.

For any incremental time period, let:

RO_1 = Pu:(U + Pu) ratio of the solid in the 1th radial increment
at the start of the time period,

RA_i = Pu:U ratio of the material added to the i th increment,

RR_i = Pu:U ratio of the material removed from the i th increment,

RF_i = Pu:(U + Pu) ratio of the i th increment at the end of the time period,

MO_i = mass of heavy metal in the i th increment at the start of the time period,

MA_i = mass of heavy metal added to the i th increment as a result of pore migration during the time period, and

MR_i = mass of heavy metal removed from the i th increment as a result of pore migration during the time period.

At the end of the time period, the Pu:(U + Pu) ratio of the i th increment is simply:

$$RF_i = \frac{MO_i (RO_i) + MA_i [RA_i / (1 + RA_i)] - MR_i [RR_i / (1 + RR_i)]}{MO_i + MA_i - MR_i} \quad (14)$$

Since $RR_i = RA_{i+1}$, and $MR_i = MA_{i+1}$, we get:

$$RF_i = \frac{MO_i (RO_i) + MA_i [RA_i / (1 + RA_i)] - MA_{i+1} [RA_{i+1} / (1 + RA_{i+1})]}{MO_i + MA_i - MA_{i+1}} \quad (15)$$

The masses are obtained from the porosity redistribution model, and RA is calculated from equilibrium thermodynamics as discussed in Appendix A. Typical values of RA (i.e., the Pu:U ratio of the vapor transported material) are plotted in Fig. 7 as a function of temperature and the oxygen-to-metal ratio of the solid. These values plus about 40 other values calculated for intermediate oxygen-to-metal ratios (see Fig. 8) were used to develop Eqs. (16) through (19), which were actually used in the computer

program. These least-squares equations give the Pu:U ratio of the vapor phase over $U_{0.8}Pu_{0.2}O_{2-x}$ as a function of temperature and plutonium valence.

$$\begin{aligned} \text{For } T > 2600: \quad RA &= 58.780 - 7.2875 \times 10^{-3} T + 3.328 \times 10^{-7} T^2 \\ &- 25.8581 V + 2.8677 V^2 + 1.5003 \times 10^{-3} TV . \end{aligned} \quad (16)$$

$$\begin{aligned} \text{For } 2200 < T < 2600: \quad RA &= 93.981 - 1.3288 \times 10^{-2} T + 6.857 \times 10^{-7} T^2 \\ &- 41.8917 V + 4.7409 V^2 + 2.7260 \times 10^{-3} TV . \end{aligned} \quad (17)$$

$$\begin{aligned} \text{For } 1800 < T < 2200: \quad RA &= 98.844 - 1.5669 \times 10^{-2} T + 5.307 \times 10^{-7} T^2 \\ &- 43.0339 V + 4.6458 V^2 + 3.5429 \times 10^{-3} TV . \end{aligned} \quad (18)$$

$$\begin{aligned} \text{For } T < 1800: \quad RA &= 103.178 - 1.3296 \times 10^{-2} T + 4.631 \times 10^{-7} T^2 \\ &- 46.6616 V + 5.2677 V^2 + 3.0177 \times 10^{-3} TV . \end{aligned} \quad (19)$$

In these equations,

RA = Pu:U ratio of the gas,

T = temperature in °K, and

V = average Pu valence of the solid.

For hypostoichiometric mixed oxide the plutonium valence is, of course, related to the oxygen-to-metal ratio and the Pu:(U + Pu) ratio, y:

$$v = [2(O/M) - 4(1 - y)]/y .$$

Equations (16) through (19) are valid for temperatures between about 1400 and 3000°K and all combinations of plutonium valence that will be encountered in fuel pins containing hypostoichiometric fuel. Stoichiometric fuel was treated as a special case. This was necessary, since the thermodynamic calculations for stoichiometric fuel at 3000°K

yielded a vapor composition that was slightly rich in plutonium compared to the solid. Since there is adequate experimental evidence that the vapor over stoichiometric mixed oxide is always rich in uranium, the thermodynamic calculations for stoichiometric fuel at the higher temperatures are unreliable. For this reason, we established the high-temperature portion of the curve shown in Fig. 7 for stoichiometric oxide by extrapolating the low-temperature results with the stipulation that the Pu:U ratio at 3000°K be 0.25. Equations (20) and (21), which describe the resulting relationship, were used in the model whenever the initial fuel was stoichiometric or whenever initially hypostoichiometric fuel increased to an oxygen-to-metal ratio of 2.00 as a result of burnup of the actinides.

$$\text{For } T > 1727: \text{ RA} = 0.6320 - 1.0909 \times 10^{-3} T + 5.566 \times 10^{-7} T^2 - 7.6232 \times 10^{-11} T^3, \quad (20)$$

$$\text{For } T < 1727: \text{ RA} = -0.03374 + 3.01167 \times 10^{-5} T, \quad (21)$$

where

RA = Pu:U ratio of the gas, and

T = temperature in °C.

Attention is called to the fact that temperature is in °K for Eqs. (16) through (19) but in °C for Eqs. (20) and (21).

Equations (16) through (21) give the vapor composition over oxide containing 20% plutonia. However, these equations can be used to predict the vapor-phase composition when the plutonia content differs from 20%, since under the assumption of an ideal solid solution, the partial pressure of the plutonium- and uranium-bearing gaseous species are

directly proportional to the mole fraction of plutonia and urania present in the solid. Therefore, Eqs. (16) through (21) are corrected in the computer program for the localized Pu:(U + Pu) ratio of the solid, RO , by multiplying each equation by the factor $4 RO_{i-1}/(1 - RO_{i-1})$. Neither Eq. (19) nor Eq. (21) is valid below about 1400°K, but at such low temperatures negligible vapor transport is predicted by the model and the vapor composition is not needed. Actually, as shown earlier, a small amount of fuel is deposited onto the cladding, but in the model we have not attempted to account for this transport of fuel.

Discussion of Gas Phase Composition

Before comparing predictions of the model with experimentally measured actinide profiles, it is informative to discuss the values calculated for the vapor-phase composition, since these calculations give evidence in addition to that previously discussed that the commonly accepted assumption^{39, 53}) of a constant $H_2O:H_2$ or $CO_2:CO$ ratio existing throughout a fuel pin is incorrect.

Originally, we planned to base oxygen redistribution on the assumption that throughout the fuel pin a constant $H_2O:H_2$ ratio existed, controlled by the overall oxygen-to-metal ratio of the fuel pin. Accordingly, the Pu:U ratio of the vapor phase was calculated for a series of fixed $H_2O:H_2$ ratios and temperatures. The results of these calculations for a solid containing 20% plutonia are plotted in Fig. 8. For any given $H_2O:H_2$ ratio and temperature it is possible to calculate an oxygen-to-metal ratio for the solid phase.³⁹) Such oxygen-to-metal ratios are shown in the figure. Each of the curves can be equated to an overall

oxygen-to-metal ratio of a fuel pin if the in-reactor temperature profile is known. For a temperature profile typical of LMFBR and GCBR fuel pins, examination of the oxygen-to-metal ratios in the figure shows that if the assumption of a constant $H_2O:H_2$ ratio were correct, the volume-averaged oxygen-to-metal ratio for the lower curve would be representative of a nearly stoichiometric fuel, while the upper curve would be representative of substantially hypostoichiometric fuel.

For the nearly stoichiometric fuel, note that the vapor is rich in uranium compared to the solid composition at all temperatures up to about $3000^\circ K$. Thus, one would expect a vaporization-condensation mechanism to result in concentration of plutonium in the center of a fuel pin and a buildup of uranium in the cooler portions of the pin, provided the central fuel temperature did not exceed about $3000^\circ K$. However, examination of the second curve from the bottom of the figure, which is representative of a fuel pin with an overall oxygen-to-metal ratio of about 1.99, indicates that above $2500^\circ K$ the evaporation-condensation mechanism would result in concentration of uranium rather than plutonium in the center of the fuel pin. Since this prediction is not in accord with numerous observations of $Pu:(U + Pu)$ profiles of irradiated fuel pins operated under conditions suitable for comparison, this is taken as evidence that the assumption of a constant $H_2O:H_2$ is invalid. Such an assumption leads to overpredicting the extent of oxygen redistribution. Since the assumption of a constant $CO_2:CO$ ratio yields practically the same oxygen-to-metal profile, it appears that oxygen redistribution (at least for hypostoichiometric fuel) cannot be described based on a constant $H_2O:H_2$ or $CO_2:CO$ ratio. Further, Leitnaker⁵⁵⁾ has performed calculations that

indicate that diffusion of hydrogen through the cladding or deposition of carbon would reduce the gas pressures to the point where oxygen transport via the $H_2O:H_2$ or $CO_2:CO$ mechanism would be negligible even for stoichiometric $(U,Pu)O_2$.

An observation that is not associated with the assumption of a constant $H_2O:H_2$ ratio is that the oxygen-to-metal ratio that yields a vapor having the same plutonium-to-uranium ratio as the solid decreases with increasing temperature, as can be seen by noting the oxygen-to-metal ratios on following the dashed line in Fig. 8 from left to right. (It is proper to use Fig. 8 in this manner since, even though the assumption of a constant $H_2O:H_2$ ratio appears incorrect, the plutonium-to-uranium ratios given are valid for the temperatures and oxygen-to-metal ratios reported in the figure.) In other words, the oxygen-to-metal ratio of the pseudocongruently vaporizing solid depends on temperature. It should be pointed out that this conclusion, as well as all others based on values calculated for the vapor phase composition, are tentative, since the calculations require extrapolation of oxygen potential and other thermodynamic data to high temperatures. Additional experimental work in this area is warranted.

Additional points that are evident from study of Figs. 7 and 8 are that for any temperature between 1800 and 3000°K the plutonium-to-uranium ratio of the vapor increases with decreasing oxygen-to-metal ratio. Also, for any fuel pin in which oxygen redistribution yields an oxygen-to-metal ratio as low as 1.94, the calculations show the vapor to be rich in plutonium, and thus uranium would be concentrated in the hotter fuel. As previously discussed, comparison with the experimental values shows the

calculations to be in general agreement with the results of Ohse and Olson;⁴⁴⁾ however, the measurement of Battles et al.⁴⁵⁾ indicates that the plutonium-to-uranium ratio of the vapor is smaller than the calculated values.

Limitations of Actinide Redistribution Model

The development of models to predict fuel behavior is a dynamic and evolutionary process. Even though we believe our current model is very valuable, we do not believe it is entirely correct and have included here some discussion of the shortcomings.

The model employs Eq. (3) for predicting the effect of oxygen-to-metal ratio on fuel thermal conductivity, and this equation is based on a limited amount of data. However, uncertainty in the thermal conductivity is not likely to be a serious shortcoming for the following reasons. The thermal conductivity equation is likely to predict reasonably accurate values for stoichiometric mixed oxides. For fuel pins initially containing stoichiometric or hypostoichiometric oxide, the cooler fuel will tend to approach an oxygen-to-metal ratio of 2.00 as a result of oxygen redistribution. Thus, for the cooler fuel, for which the stoichiometry effect is most prominent, the conductivity equation employed should yield reasonable values. The hotter fuel may be appreciably hypostoichiometric, but extrapolation of the results of Gibby⁸⁾ and Laskiewicz et al.¹⁰⁾ indicates that conductivity is relatively insensitive to stoichiometry above about 1500°C. Second, the model does not account for the small effect that variations in the Pu:(U + Pu) ratio will have on low-temperature conductivity.³⁾ Above about 1200°C this

could be negligible since the two attempts^{3,10)} to measure the effect of plutonium content on conductivity at temperatures above 1200°C have shown the magnitude of the effect to be within the measurement error. A third and perhaps more serious shortcoming, for which no solution is currently available, is our inability to correct the conductivity of the fuel for the effect of pore shape in the as-fabricated fuel and the changes in pore shape that occur during in-reactor restructuring. It has been shown,^{56,57)} at least for pellets fabricated by the high-pressure pre-slug technique, that pore morphology can cause variations in conductivity of 30 to 40% at 1500°C and lower. The effect becomes less important with increasing temperature.

Another potential shortcoming of the model is that it does not provide for actinide redistribution via solid-state diffusion (i.e., the Soret effect). Similarly, ordinary solid-state chemical diffusion of uranium and plutonium that would oppose any segregation has not been included in the model. The importance of these two effects is unknown.

Comparison of Measured and Predicted Actinide Distribution

An experimentally measured actinide radial distribution for one of the fuel pins previously described (43-112-3) is compared in Fig. 9 with the distribution predicted using the model. Over the range for which experimental measurements are available, the agreement is very good. Although experimental data are not available for comparison over the remainder of the cross section, the shape of the predicted profile is very similar to those observed by others³⁰⁾ for pins that also did not experience fuel melting. Comparisons of measured and predicted profiles

for other fuel pins having different fabrication and irradiation conditions are necessary to determine the validity of the model, but these initial calculations are encouraging.

SUMMARY

1. An analytical model based on the evaporation-condensation mechanism of material transport was developed and shown to adequately describe the radial porosity distribution resulting from irradiation of $(U,Pu)O_2$.

2. The volume-averaged porosity of the columnar grain region of $(U,Pu)O_2$ fuel pins was 5.9 and $\geq 3.8\%$ after irradiation to burnups of 0.7 and 4.2% FIMA, respectively. The result of these higher than expected values is an increase in central fuel temperatures.

3. Actinide redistribution in stoichiometric $(U,Pu)O_2$ occurs via the evaporation-condensation mechanism, which increases the $Pu:(U + Pu)$ of the hotter fuel. Indications are that this mechanism would lead to decreased $Pu:(U + Pu)$ values for markedly hypostoichiometric fuel, but thermally induced solid-state migration of the actinides may or may not nullify such segregation or might lead to increased $Pu:(U + Pu)$ ratios for the hotter fuel. In-reactor tests and out-of-reactor radial temperature-gradient tests of the effects of stoichiometry, porosity, and irradiation time on actinide redistribution are needed.

4. A kinetic actinide redistribution model based on vapor phase transport was developed and shown to accurately predict the radial $Pu:(U + Pu)$ profile for an irradiated fuel pin containing stoichiometric fuel.

ACKNOWLEDGMENTS

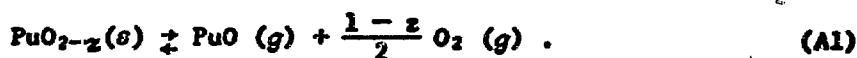
The metallography was performed by L. G. Shrader and E. R. Boyd under the direction of E. L. Long, Jr. T. M. Kegley, Jr., performed the Quantimet porosity determinations. The assistance of J. H. Coobs, T. B. Lindemer, and S. Peterson in reviewing the manuscript is gratefully acknowledged.

APPENDIX A

Calculation of Gas Phase Composition and Pressure
in Equilibrium with $U_{0.8}Pu_{0.2}O_{2-x}$

To calculate the composition and pressure of the gas phase it is assumed that the vapor is in isothermal thermodynamic equilibrium with single-phase solid $U_{1-y}Pu_yO_{2-yz}$. It is further assumed that the solid solution is ideal - that is, the solid solution behaves as a mixture of $1-y$ moles of UO_2 and y moles of PuO_{2-z} . The available experimental evidence³⁹⁻⁵⁸⁾ indicates that the assumption of a single-phase ideal solid solution is reasonable. Each of the vapor species (U , UO , UO_2 , UO_3 , Pu , PuO , and PuO_2) is formed by either decomposition or sublimation of $UO_2(s)$ or $PuO_{2-z}(s)$ or by reaction of these solids with oxygen. Basically the same procedure is used to calculate the partial pressure of each vapor species, and calculation of the partial pressure of $PuO(g)$ is presented here as an example. Except where specifically noted, all thermodynamic data were obtained from the compilation of Rand and Marink.³⁹⁾

The reaction that yields $PuO(g)$ is



At equilibrium

$$\Delta G = 0 = \Delta G^\circ + RT \ln \frac{(P_{PuO})(P_{O_2})^{\frac{1-z}{2}}}{y} \quad (A2)$$

where

ΔG° = standard free energy of the reaction,

P_i = partial pressure of species i,

y = mole fraction of plutonia in the solid,

T = temperature, °K, and

R = gas constant (1.987 cal mole⁻¹ °K⁻¹).

Rearrangement of Eq. (A2) yields the vapor pressure of PuO(g):

$$P_{\text{PuO}} = -\frac{\Delta G^\circ}{RT} - \frac{1-z}{2} \ln P_{\text{O}_2} + \ln y \quad (\text{A3})$$

The value of ΔG° is obtained by subtracting the standard free energy of formation of the reactants from that of the products. A complicating factor is that the free energy of formation of $\text{PuO}_{2-z}(\text{s})$ depends on the stoichiometry. For a given value of z the free energy of formation of $\text{PuO}_{2-z}(\text{c})$ is customarily given as a function of temperature by an equation of the form

$$\Delta G_f^\circ = A + BT \quad (\text{A4})$$

where

ΔG_f° = free energy of formation, cal/mole,

T = temperature, °K, and

A, B = stoichiometry dependent constants.

By least-squares analysis Eqs. (A5) and (A6) were developed to yield

A and B as functions of z:

$$A = [86.7941 - 423.07(2 - z) + 233.547(2 - z)^2 - 53.0113(2 - z)^3](10^3) \quad (\text{A5})$$

$$B = -121.263 + 324(2 - z) - 228.926(2 - z)^2 + 53.6287(2 - z)^3 \quad (A6)$$

Before Eq. (A3) can be used to calculate the pressure of PuO a value for P_{O_2} must be obtained. For a given oxygen-to-metal ratio of the solid the oxygen pressure can be obtained from available tabulations⁵⁹⁾ of oxygen potentials over the solid of interest or by extrapolation of these values to the temperature of interest. The extrapolations were conducted by fitting the tabulated oxygen potentials to equations of the following form:

$$\Delta\bar{G} = a + bT + cT^2, \quad (A7)$$

where

$\Delta\bar{G}$ = oxygen potential, kcal/mole,

a, b, c = stoichiometry dependent constants, and

T = temperature, °K.

An equation of this type was used for each of six levels of plutonium valence in the range 3.00 to 3.98. These equations were then used to obtain oxygen potentials at temperatures up to 3000°K. The coefficients for Eq. (A7) are given in Table A-1. With the limitation that the equation for a plutonium valence of 3.98 predicts poorly above 2800°K, we believe these equations, which are based on the measurements of Markin and McIver,⁶⁰⁾ represent the best available oxygen potential values for hypostoichiometric $(\text{U}, \text{Pu})\text{O}_2$. We considered use of the oxygen potential values determined by others^{61, 62)} but chose the work of Markin and McIver, since one of the other two studies gave oxygen potentials smaller than the extrapolated values of Markin and McIver, but the second study

Table A-1. Coefficients for Eq. (A7) Used in Calculating Oxygen Potential as a Function of Temperature

Plutonium Valence	Coefficients		
	a	b × 10 ²	c × 10 ⁶
3.98	186.357	-6.001	7.8125
3.30	198.214	-5.741	5.80357
3.60	197.143	-4.510	2.00893
3.40	205.571	-4.879	4.24107
3.20	214.786	-5.435	6.47321
3.00	217.500	-5.00446	5.13393

gave larger values. Rather than specifying initial stoichiometry of the solid it is also possible to specify a H₂O:H₂ or CO₂:CO ratio with which the solid is in equilibrium. With this alternative approach one first calculates the oxygen potential based on the dissociation of H₂O or CO₂ and then the oxygen-to-metal ratio of the solid. To calculate the oxygen-to-metal ratio it is necessary to have a relationship between the plutonium valence and the oxygen potential for each temperature of interest. Such equations were obtained by least-squares analysis of the tabulated³⁹⁾ and extrapolated oxygen potential values mentioned earlier. Each equation was of the form

$$V = A + B(\overline{\Delta G}) + C(\overline{\Delta G})^2 + D(\overline{\Delta G})^3 + E(\overline{\Delta G})^4, \quad (A8)$$

where

- V = plutonium valence at the temperature of interest,
- A, B, C, D, E = coefficients determined by regression analysis, and
- $\overline{\Delta G}$ = oxygen potential, kcal/mole.

Values for the regression coefficients are given in Table A-2 for temperatures between 1000 and 3000°K.

Regardless of whether the oxygen-to-metal ratio of the solid or the $H_2O:H_2$ or $CO_2:CO$ ratio in equilibrium with the solid was specified, Eq. (A3) was used to calculate the partial pressure of $PuO(g)$ once the oxygen potential was obtained. The vapor pressure calculations are quite time consuming if performed by hand and thus were performed with the aid of a computer. The calculational procedure was verified by reproducing the portion of Fig. 1 in Rand and Markin's report³⁹⁾ for hypostoichiometric oxide.

Table A-2. Regression Coefficients for Eq. (A8)

Temperature (°K)	A	B	C	D	E
1000	-1.1492	0.0880643	-3.71263E-4	0	0
1200	0.507513	0.068163	-3.22158E-4	0	0
1400	0.635936	0.068007	-3.36449E-4	0	0
1600	2.30106	0.0442139	-2.63125E-4	0	0
1800	3.35988	0.0275037	-2.07911E-4	0	0
2000	4.1002	0.0146168	-1.63027E-4	0	0
2200	78.0375	-2.3796	0.028293	-1.47033E-4	2.7756E-7
2400	-116.472	4.87525	-0.0728613	4.77513E-4	-1.16334E-6
2600	-30.5881	1.79813	-3.24343E-2	2.47021E-4	-6.84264E-7
2800	24.7801	-0.489513	0.00206175	2.11142E-5	-1.41412E-7
3000	-40.9632	2.38732	-4.53436E-2	3.68486E-4	-1.0944E-6

APPENDIX B

Effect of Stoichiometry on the Vapor Pressure of $(U,Pu)O_{2-x}$

It is generally agreed that the vapor pressure of a hypostoichiometric urania-plutonia solid solution is less than that of the stoichiometric material. To get an indication of the significance of the reduced vapor pressure of the low oxygen-to-metal ratio fuel on the extent of restructuring and consequently also on the extent of actinide redistribution, the total vapor pressure was calculated for oxygen-to-metal ratios over the range 1.94 to 2.00. The results of these calculations are given in Fig. 10. The upper curve gives the calculated vapor pressure for stoichiometric material. The lower two curves show calculated pressures for oxygen-to-metal ratios of 1.98 and 1.94. The calculated values compare favorably with the experimental results of Ohse and Olson;⁴⁴⁾ the measurements of Battles et al.⁴⁵⁾ show the pressure to increase more rapidly with increasing oxygen-to-metal ratio. For the purpose of estimating the effect that the reduced vapor pressure would have on the extent of restructuring in fuels with low oxygen-to-metal ratios, consider the values at 2200°K. The upper curve shows that the vapor pressure over the stoichiometric fuel is about 10^{-5} atm. We can see from the lower curve that to have this pressure over fuel with an oxygen-to-metal ratio of 1.94 requires increasing the temperature to about 2300°K; that is, there is about a 100° effect. The experimental data of Battles et al.⁴⁵⁾ indicate a 200° effect. At higher temperatures the curves are closer together, indicating that the vapor pressure is not as dependent on the oxygen-to-metal ratio. It appears that, although there is not a

sufficiently large effect to completely prevent actinide redistribution via the vapor phase mechanism, low oxygen-to-metal ratio fuel should experience a measurable reduction in the extent of redistribution, and the rate of pore migration should also be slowed.

Table 1. Actinide Redistribution in Fuel with Low Oxygen-to-Metal Ratio^a

Oxygen-to-Metal Ratio	In-Reactor or Out-of-Reactor	Time (hr)	Maximum Temperature (°C)	Change in Plutonium Content of Hottest Fuel	Reference
1.93	Out-of-reactor	48	2470	Increased	32
1.95	In-reactor	b	Not reported	Increased	46
1.96	Out-of-reactor	1	2400	Unchanged	35
1.97	Out-of-reactor	1	2400	Increased	35

^aIrradiation and out-of-reactor tests of fuel with oxygen-to-metal ratios of 1.98 and larger show an increase in the Pu:(U + Pu) ratio of the hotter fuel. The extent of the segregation increases with the oxygen-to-metal ratio.

^bNot reported, but several days, since the burnup was 8000 MWd/metric ton.

REFERENCES

- 1) W. E. Baily, E. A. Aitken, R. R. Asamoto, and C. N. Craig, "Thermal Conductivity of Uranium-Plutonium Oxide Fuels," pp. 293-308 in *Intern. Symp. Plutonium Fuels Technol., Scottsdale, Arizona, 1967, Nucl. Met. 13*, American Institute of Mining, Metallurgical, and Petroleum Engineers, New York, 1968.
- 2) R. R. Asamoto, F. L. Anselin, and A. E. Conti, *J. Nucl. Mater.* 29 (1969) 67-81.
- 3) R. L. Gibby, *J. Nucl. Mater.* 38 (1971) 163-177.
- 4) B. F. Rubin, General Electric (USA) Report, GEAP 13582 (1970).
- 5) H. E. Schmidt and J. Richter, "The Influence of Stoichiometry on the Thermal Conductivity of $(U_{0.8}, Pu_{0.2})O_{2+x}$," paper presented at the Oxide Fuel Thermal Conductivity Symposium, Stockholm, Sweden, June 1, 1967.
- 6) F. J. Hetzler, T. E. Lannin, K. J. Perry and E. L. Zebroski, General Electric (USA) Report, GEAP 4879 (1967).
- 7) J. A. Christensen, *Trans. Am. Nucl. Soc.* 11 (1968) 131.
- 8) R. L. Gibby, Battelle (USA) Report, BNWL 927 (1969).
- 9) *Sodium-Cooled Reactors, Fast Ceramic Reactor Development Program*, General Electric (USA) Report, GEAP 10028-35 (1970) 44-49.
- 10) R. A. Laskiewicz, G. F. Melde, S. K. Evans, and P. E. Bohaboy, General Electric (USA) Report, GEAP 13733 (1971).
- 11) W. T. Sha, P. R. Heubotter, and R. K. Lo, *Trans. Am. Nucl. Soc.* 14 (1971) 183-184.
- 12) W. L. Lyon and W. E. Baily, *J. Nucl. Mater.* 22 (1967) 332-339.
- 13) E. A. Aitken and S. K. Evans, General Electric (USA) Report, GEAP 5672 (1968).

- 14) F. J. Homan, C. M. Cox, and W. J. Lackey, "Comparisons between Predicted and Measured Fuel Pin Performance," pp. 243-258 in *Proc. Conf. Fast Reactor Fuel Element Technology*, American Nuclear Society, Hinsdale, Illinois, 1971, also ORNL TM 3386 (1971).
- 15) F. J. Homan, Oak Ridge (USA) Report, ORNL TM 3508 (1971).
- 16) J. R. MacEwan and V. B. Lawson, *J. Am. Ceram. Soc.* 45 (1962) 42-46.
- 17) D. R. de Halas and G. R. Horn, *J. Nucl. Mater.* 8 (1963) 207-220.
- 18) F. A. Nichols, *J. Nucl. Mater.* 22 (1967) 214-222.
- 19) A. R. Olsen, R. B. Fitts, and W. J. Lackey, "In-Reactor Restructuring Temperatures and Kinetics for (U,Pu)O₂," pp. 579-602 in *Proc. Conf. Fast Reactor Fuel Element Technology*, American Nuclear Society, Hinsdale, Illinois, 1971.
- 20) R. S. Barnes and R. S. Nelson, *Proc. Brit. Ceram. Soc.* 7 (1967) 343-353.
- 21) M.C.J. Carlson, Hanford (USA) Report, HEDL-TME (1971) 71-45.
- 22) D. P. Hines, S. Oldberg, and E. L. Zebroski, *Nucl. Appl. & Technol.* 9 (1970) 338-345.
- 23) D. C. Bullington and R. D. Leggett, "Fission-Gas Bubble Precipitation and Growth in PuO₂-UO₂ under Irradiation," pp. 545-553 in *Proceedings of the 4th International Conference on Plutonium and other Actinides, 1970*.
- 24) C. M. Cox and F. J. Homan, Oak Ridge (USA) Report, ORNL TM 2443 (1969) Addendum.
- 25) C. S. Rim and H. Fenech, *Trans. Am. Nucl. Soc.* 12 (1969) 103-104.

- 26) C. P. Ruiz, J. M. Gerhart, H. W. Alter, and L. F. Epstein, *Trans. Am. Nucl. Soc.* 6 (1963) 82-83.
- 27) T. A. Lauritzen, P. E. Novak, and J. H. Davies, General Electric (USA) Report, GEAP 4466 (1966).
- 28) D. R. O'Boyle, F. L. Brown, and J. E. Sanecki, *J. Nucl. Mater.* 29 (1969) 27-42.
- 29) N. R. Stalica and C. A. Seils, "Electron Probe Microanalysis of Irradiated Oxide Fuels," pp. 211-224 in *Proc. Intern. Symp. Ceramic Nuclear Fuels*, American Ceramic Society, Washington, D.C., 1969.
- 30) R. O. Meyer and D. R. O'Boyle, Argonne (USA) Report, ANL 7900 (1971) 5.13-5.15.
- 31) H. Beisswenger, M. Bober, and G. Schumacher, "Thermal Diffusion in UO_2 - PuO_2 Mixtures," pp. 273-282 in *Proceedings of IAEA Symposium on Plutonium as a Reactor Fuel*, Vienna, 1967.
- 32) M. Bober, C. Sari, and G. Schumacher, *Trans. Am. Nucl. Soc.* 12 (1969) 603.
- 33) M. G. Chasanov and D. F. Fischer, Argonne (USA) Report, ANL-7703 (1970).
- 34) M. Bober, C. Sari, and G. Schumacher, *J. Nucl. Mater.* 39 (1971) 265-284.
- 35) M. Bober, C. Sari, and G. Schumacher, *J. Nucl. Mater.* 40 (1971) 341-345.
- 36) *Sodium-Cooled Reactors, Fast Ceramic Reactor Development Program*, General Electric (USA) Report, GEAP 10028 35 (1970) 50-64.
- 37) G. F. Melde, T. E. Lannin, R. C. Wolf, and D. A. Cantley, *Am. Ceram. Soc. Bull.* 50 (1970) 427, also General Electric (USA) Report, GEAP 10028 36 (1970) 48-55.

- ³⁸⁾ C. P. Ruiz, J. M. Gerhart, H. W. Alter, and L. F. Epstein, Trans. Am. Nucl. Soc. 6 (1963) 83.
- ³⁹⁾ M. H. Rand and T. L. Markin, "Some Thermodynamic Aspects of (U,Pu)O₂ Solid Solutions and their Use as Nuclear Fuels," pp. 637-650 in *Thermodynamics of Nuclear Materials, 1967*, International Atomic Energy Agency, Vienna, 1968, also AERE R-5560 (1967).
- ⁴⁰⁾ E. A. Aitken and S. K. Evans, "Thermodynamic Behavior of Plutonium Oxide Systems in a Temperature Gradient," pp. 772-780 in *Proceedings of the 4th International Conference on Plutonium and Other Actinides*, 1970.
- ⁴¹⁾ E. A. Aitken and S. K. Evans, General Electric (USA) Report, GEAP 12027 (1969).
- ⁴²⁾ W. J. Lackey, A. R. Olsen, J. L. Miller, Jr., and D. K. Bates, Trans. Am. Nucl. Soc. 14 (1971) 180-182.
- ⁴³⁾ M. G. Adamson and E. A. Aitken, Trans. Am. Nucl. Soc. 14 (1971) 179-180.
- ⁴⁴⁾ R. W. Ohse and W. M. Olson, "Evaporation Behavior of Substoichiometric (U,Pu)O₂," pp. 743-752 in *Proceedings of the 4th International Conference on Plutonium and Other Actinides*, 1970, also EUR-4633e, Joint Nuclear Research Centre, Karlsruhe Establishment, Germany, 1971.
- ⁴⁵⁾ J. E. Battles, W. A. Shim, P. E. Blackburn, and R. K. Edwards, "A Mass Spectrometric Investigation of (U_{0.8},Pu_{0.2})O_{2-x}," pp. 733-742 in *Proceedings of the 4th International Conference on Plutonium and Other Actinides*, 1970.

46) H. Holleck and H. Kleykamp, Karlsruhe Nuclear Research Center, EURFNR-836 (1970).

47) J. A. Christensen, "Transport Processes in Oxide Nuclear Fuels," pp. 109-125 in *Proc. Intern. Symp. Ceramic Nuclear Fuels*, American Ceramic Society, Washington, D.C., 1969, also Battelle (USA) Report, BNWL 1202.

48) *Sodium-Cooled Reactors, Fast Ceramic Reactor Development Program*, General Electric (USA) Report, GEAP 10028 36 (1970) pp. 57-60.

49) S. K. Evans, E. A. Aitken, and C. N. Craig, *J. Nucl. Mater.* 30 (1969) 57-61.

50) E. A. Aitken, *J. Nucl. Mater.* 30 (1969) 62-73.

51) M. G. Adamson and R.F.A. Carney, *Trans. Am. Nucl. Soc.* 14 (1971) 179.

52) E. A. Aitken, S. K. Evans, M. G. Adamson, and T. E. Ludlow, General Electric (USA) Report, GEAP 12210 (1971).

53) M. H. Rand and L.E.J. Roberts, pp. 3-31 in *Proceedings on Thermodynamics of Nuclear Fuels*, International Atomic Energy Agency, Vienna, 1966.

54) W. J. Lackey, Oak Ridge (USA) Report, ORNL 4560 (1970) pp. 71-74.

55) J. M. Leitnaker, Oak Ridge (USA) Report, ORNL TM 3703 (1971) pp. 13-18.

56) R. L. Gibby and L. A. Lawrence, *Am. Ceram. Soc. Bull.* 50 (1971) 788.

57) L. A. Lawrence, R. L. Gibby, J. A. Christensen, and E. T. Weber, *Trans. Am. Nucl. Soc.* 14 (1971) 598.

⁵⁸⁾ E. A. Aitken and S. K. Evans, General Electric (USA) Report, GEAP 12153 (1970).

⁵⁹⁾ K. E. Spear, A. R. Olsen, and J. M. Leitnaker, Oak Ridge (USA) Report, ORNL TN 2494 (1969).

⁶⁰⁾ T. L. Markin and E. J. McIver, "Thermodynamic and Phase Studies for Plutonium and Uranium-Plutonium Oxides with Application to Compatibility Calculations," pp. 845-857 in *Proceedings of the 3rd International Conference on Plutonium, London, 1965*, ed. by A. E. Kay and M. B. Waldron, Chapman and Hall, 1965.

⁶¹⁾ R. E. Woodley, Am. Ceram. Soc. Bull. 50 (1971) 776.

⁶²⁾ N. A. Javed and A. A. Solomon, Am. Ceram. Soc. Bull. 50 (1971) 425.

LIST OF FIGURES

Fig. 1. Dendrites of Fuel Deposited on the Inner Surface of Microspheres Located at the Region of Transition from Columnar to Equiaxed Grains.

Fig. 2. Photomicrograph and Alpha-Autoradiograph of $U_{0.85}Pu_{0.15}O_{2.00}$ Fuel Pin 43-115-4 Showing Increased Plutonium Content Adjacent to the Central Void and Decreased Plutonium Content of the Material Vapor Deposited Between the Microspheres Located in the Cooler Portion of the Columnar Grain Region.

Fig. 3. Comparison of the Predicted and Measured Radial Porosity Distribution for $U_{0.85}Pu_{0.15}O_{2.00}$ Fuel Pin 43-112-3 Irradiated at 13.6 kW/ft to 0.7% FIMA. Unetched.

Fig. 4. Micrographs and Measured Porosity Distribution for $U_{0.85}Pu_{0.15}O_{2.00}$ Irradiated at 13.4 kW/ft to 4.2% FIMA. (a) Unetched, (b) etched.

Fig. 5. Micrograph of $U_{0.8}Pu_{0.2}O_{1.99}$ Fuel Pin S-1-E, which was irradiated in a Fast Neutron Flux at 13.5 kW/ft to 5.7% FIMA. The porosity distribution appears very similar to that of the pin shown in Fig. 4, which was irradiated in a thermal flux. Unetched.

Fig. 6. Comparison of Fuel Temperatures Calculated from the Measured and Assumed Porosity Distribution.

Fig. 7. Effect of Temperature and Stoichiometry on the Pu:U Ratio of the Gas Phase Over $U_{0.8}Pu_{0.2}O_{2-x}$. The curves were calculated with equilibrium thermodynamic. Experimentally measured values are shown for comparison. The measurements of Ohse and Olson were made with $U_{0.85}Pu_{0.15}O_{2-x}$. Their values were adjusted for the lower plutonium content by assuming that the partial pressures of uranium- and plutonium-bearing gas species were directly proportional to the mole fractions of urania and plutonia, respectively.

Fig. 8. Ratio of Pu:U in the Gas Phase Over $U_{0.8}Pu_{0.2}O_{2-x}$ as a Function of Temperature for Six $H_2O:H_2$ Ratios. The values of $2-x$ are shown beside each point in the figure.

Fig. 9. Comparison of Measured and Predicted Pu:(U + Pu) Profile for $U_{0.85}Pu_{0.15}O_{2.00}$ Fuel Pin 43-112-3 Irradiated at 13.6 kW/ft to 0.7% FIMA.

Fig. 10. Effect of Oxygen-to-Metal Ratio and Temperature on the Vapor Pressure of $U_{0.8}Pu_{0.2}O_{2-x}$.

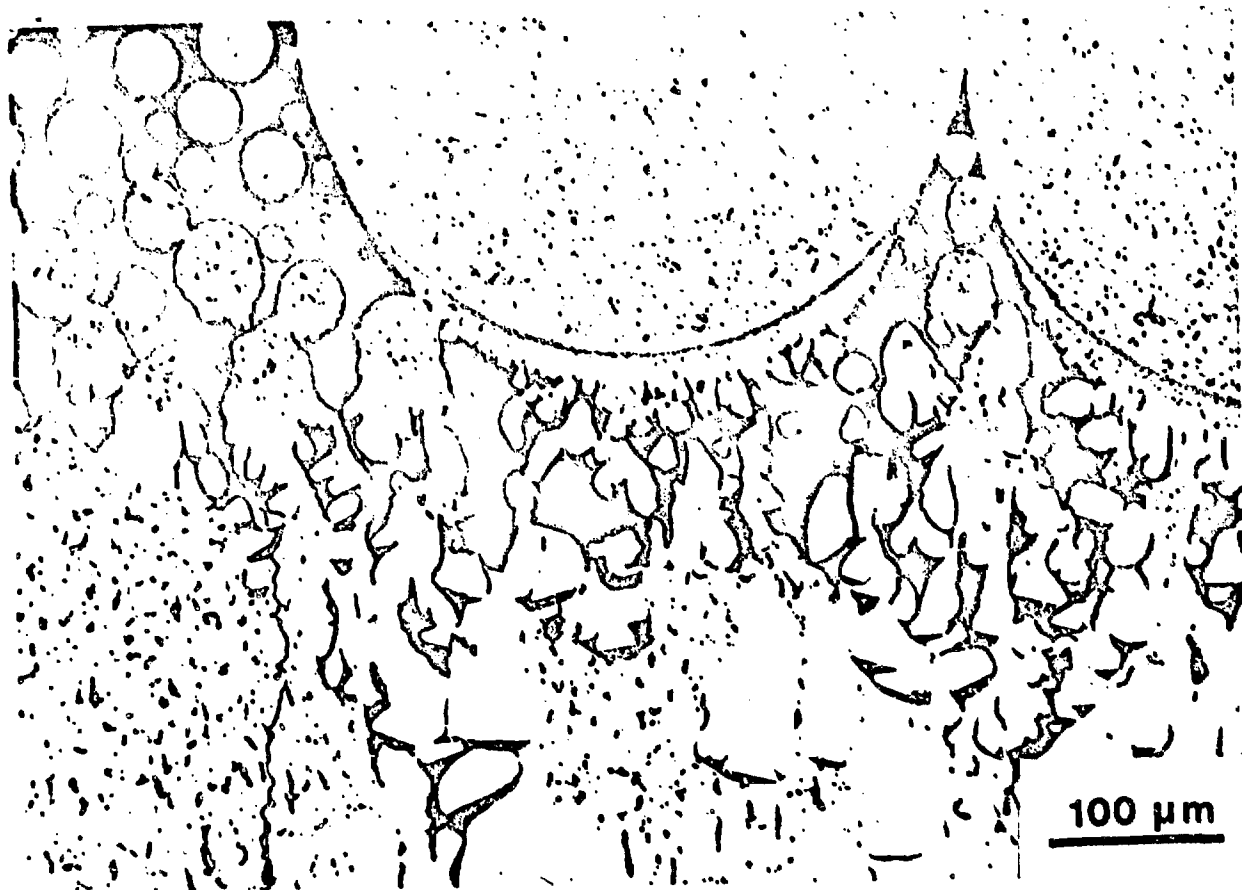
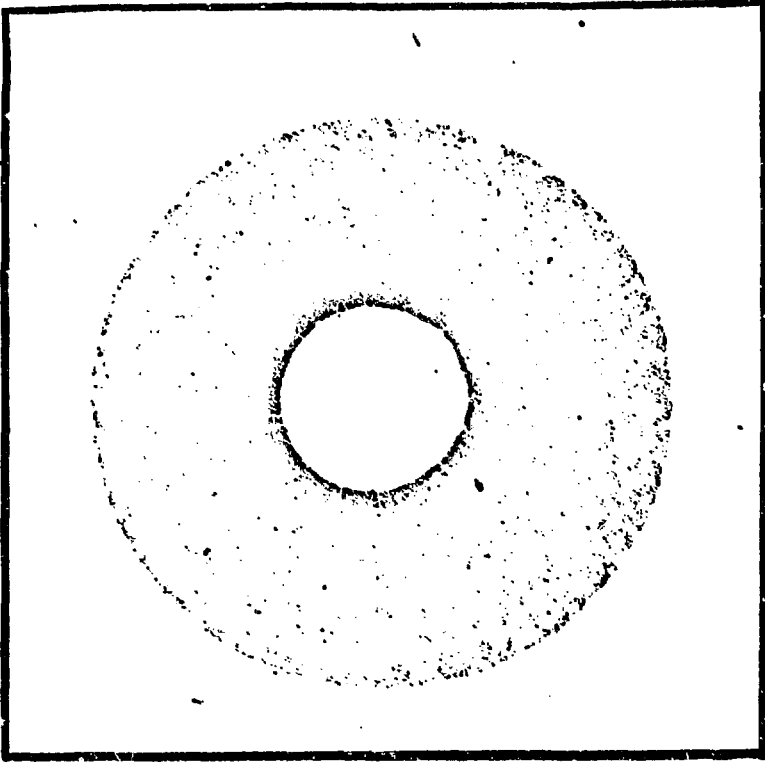


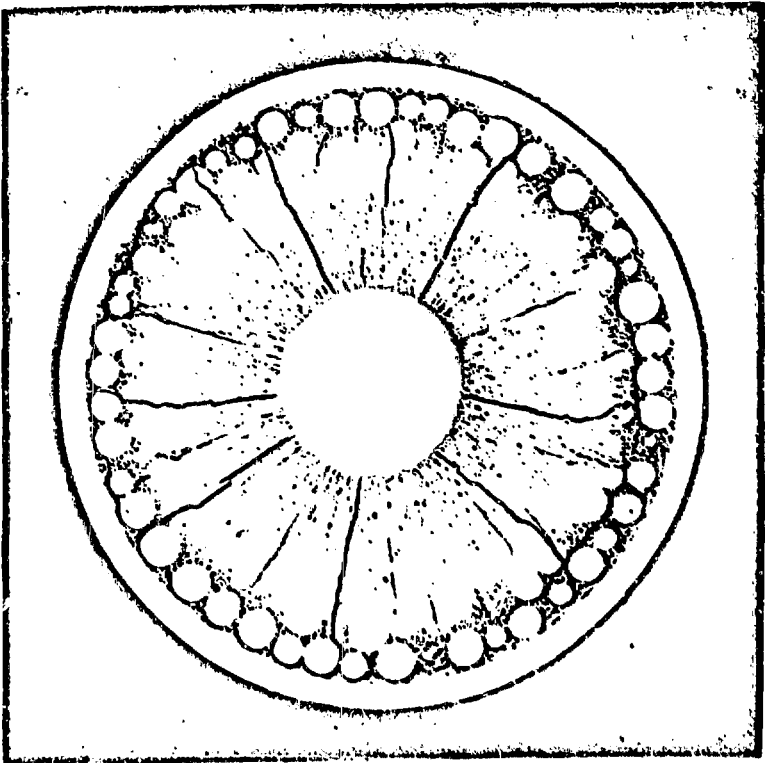
Fig. 1

R-53574



α AUTORADIOGRAPH

0.25 in



PHOTOMICROGRAPH

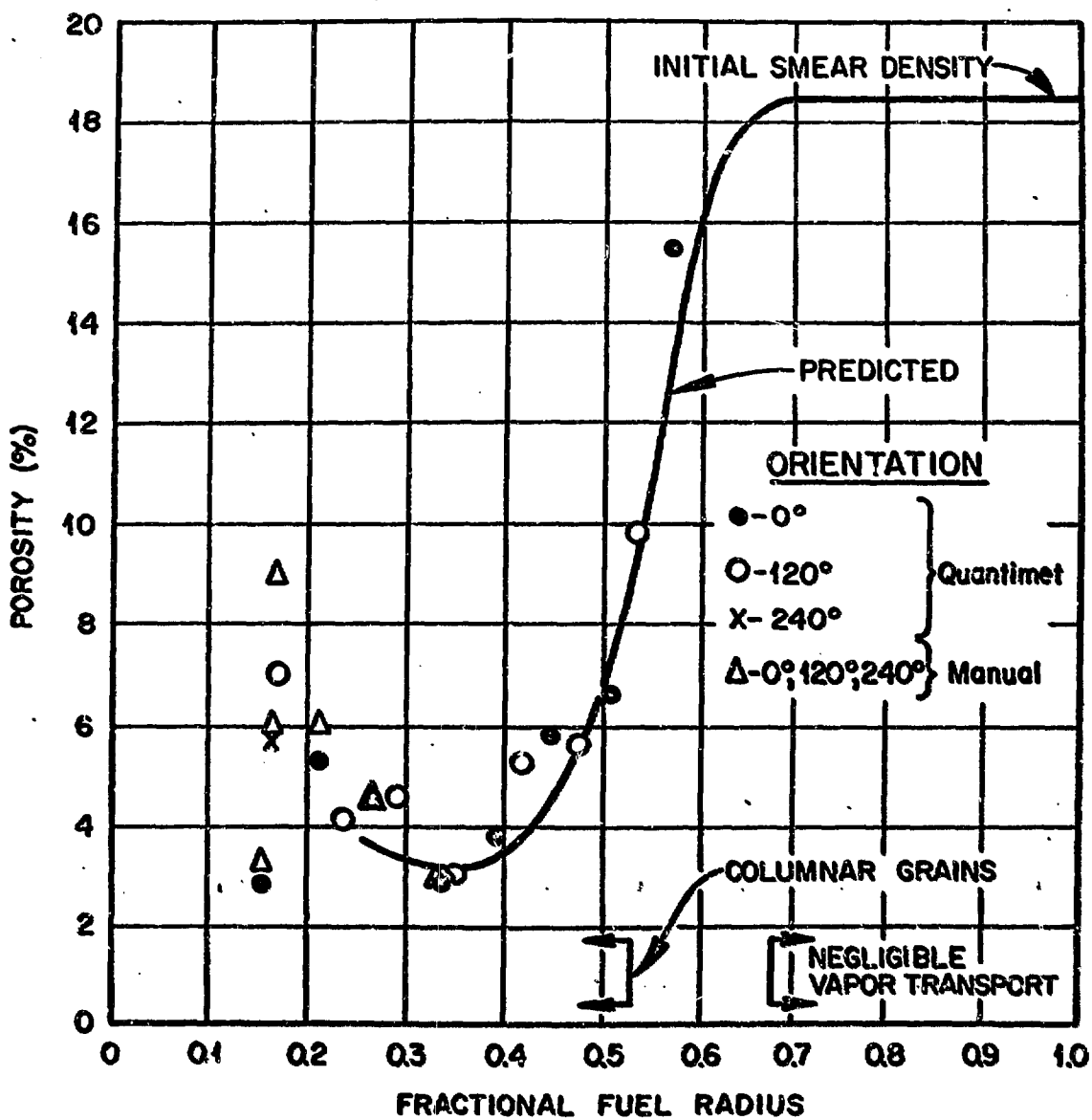
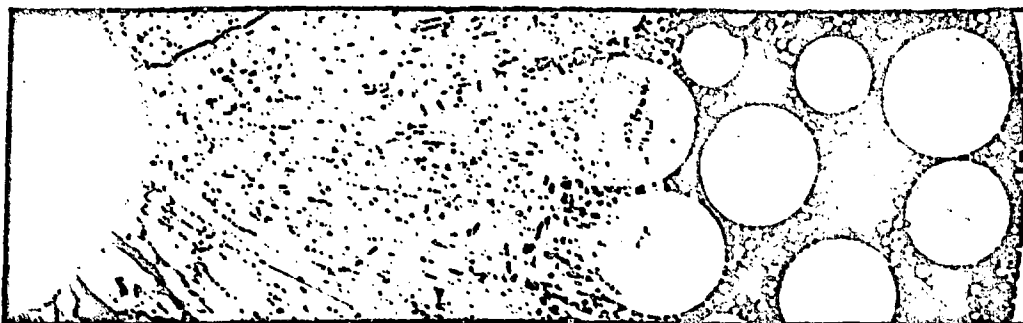
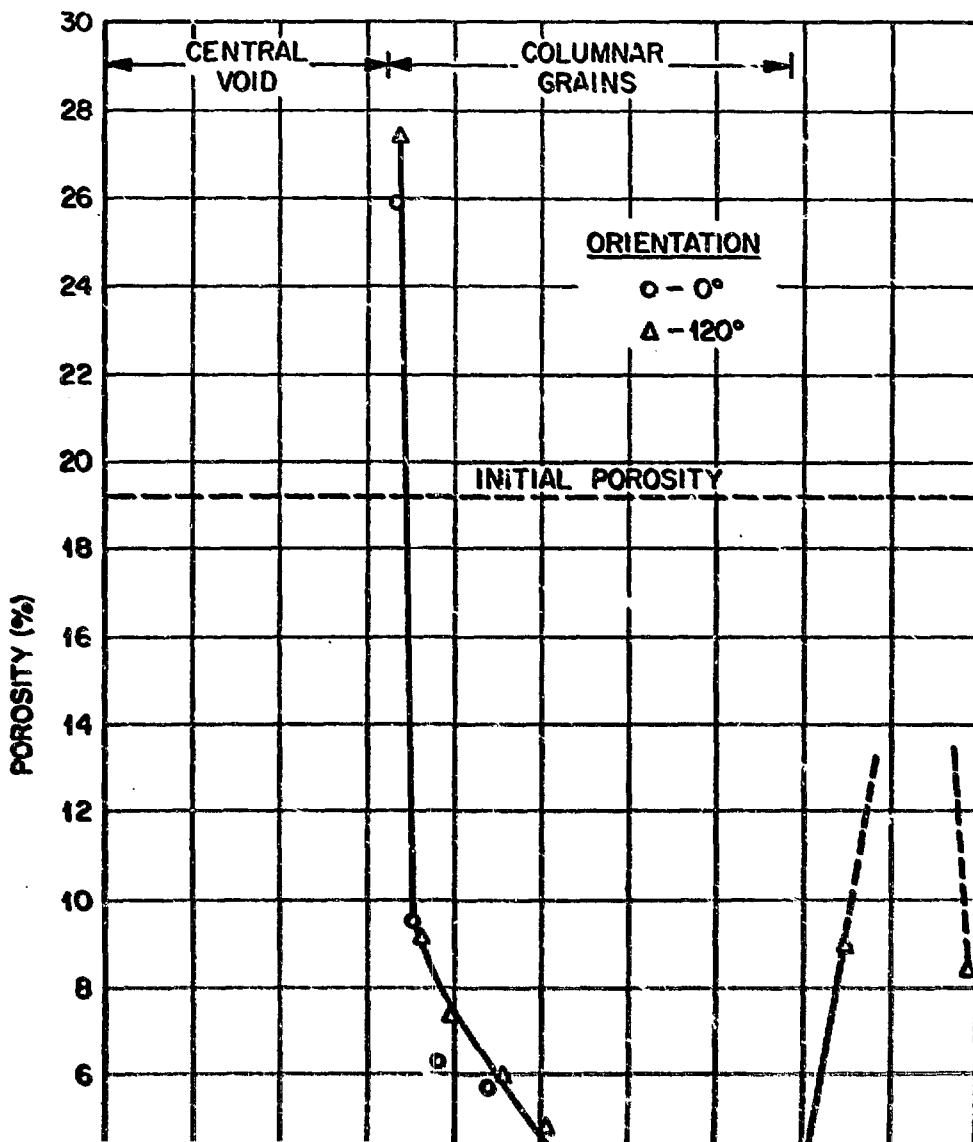


Fig. 3



ORNL-DWG 71-1054t



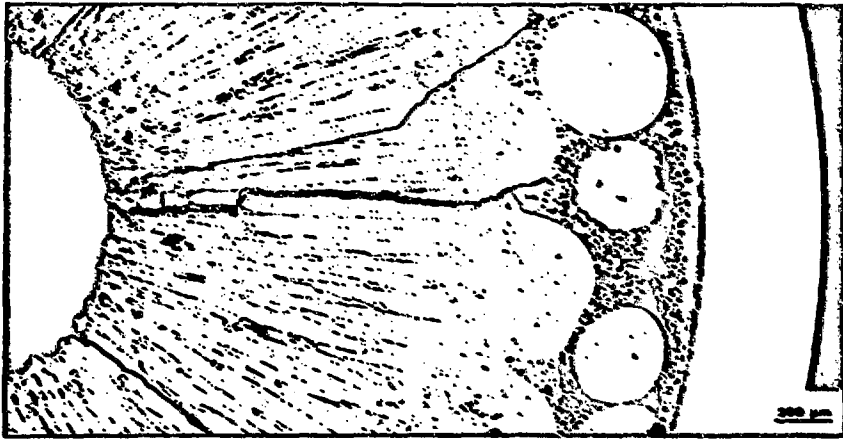


Fig. 5

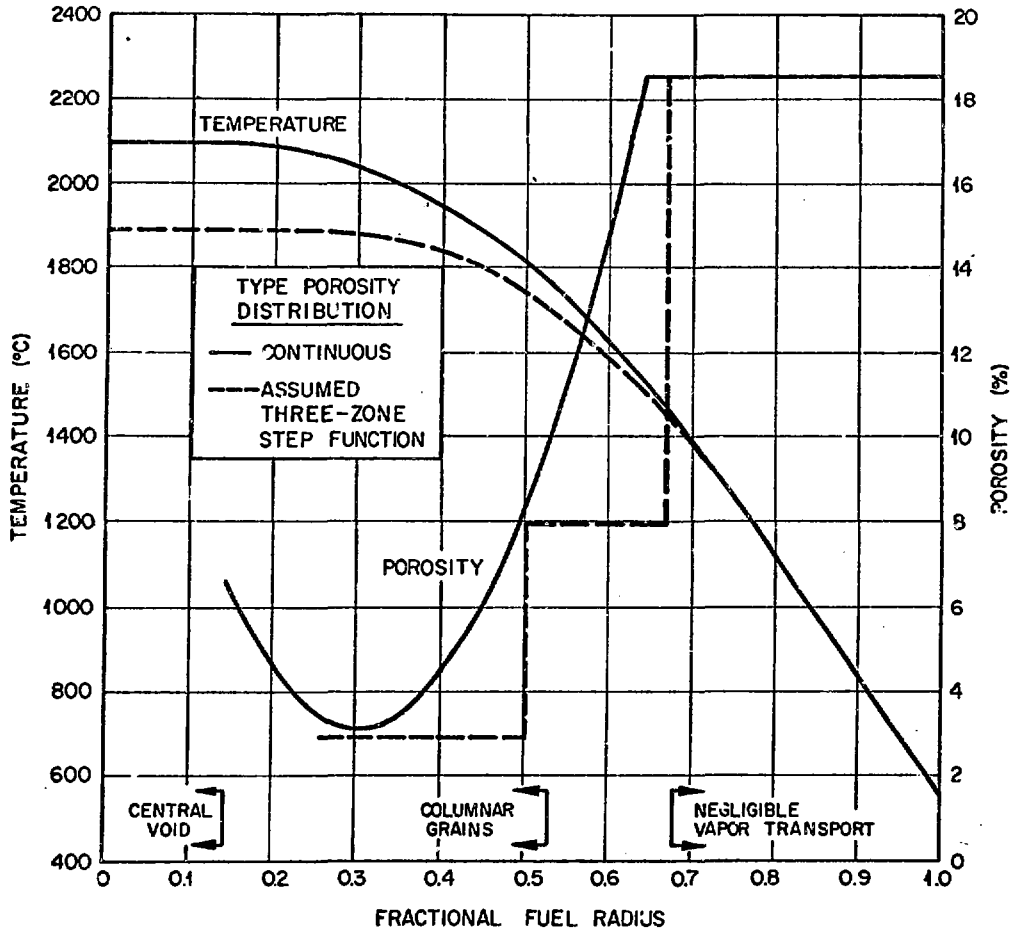


Fig. 6

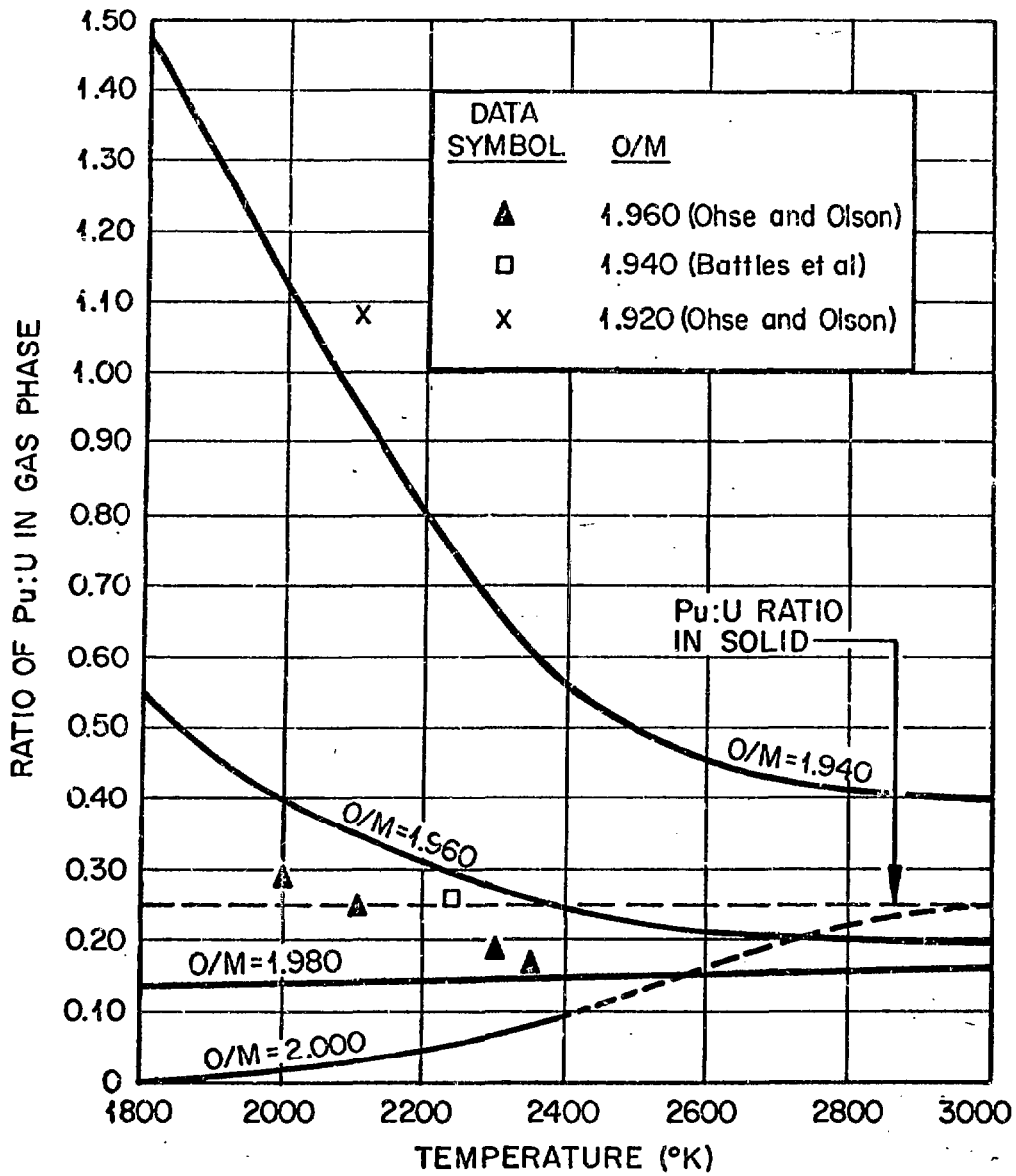


Fig. 7

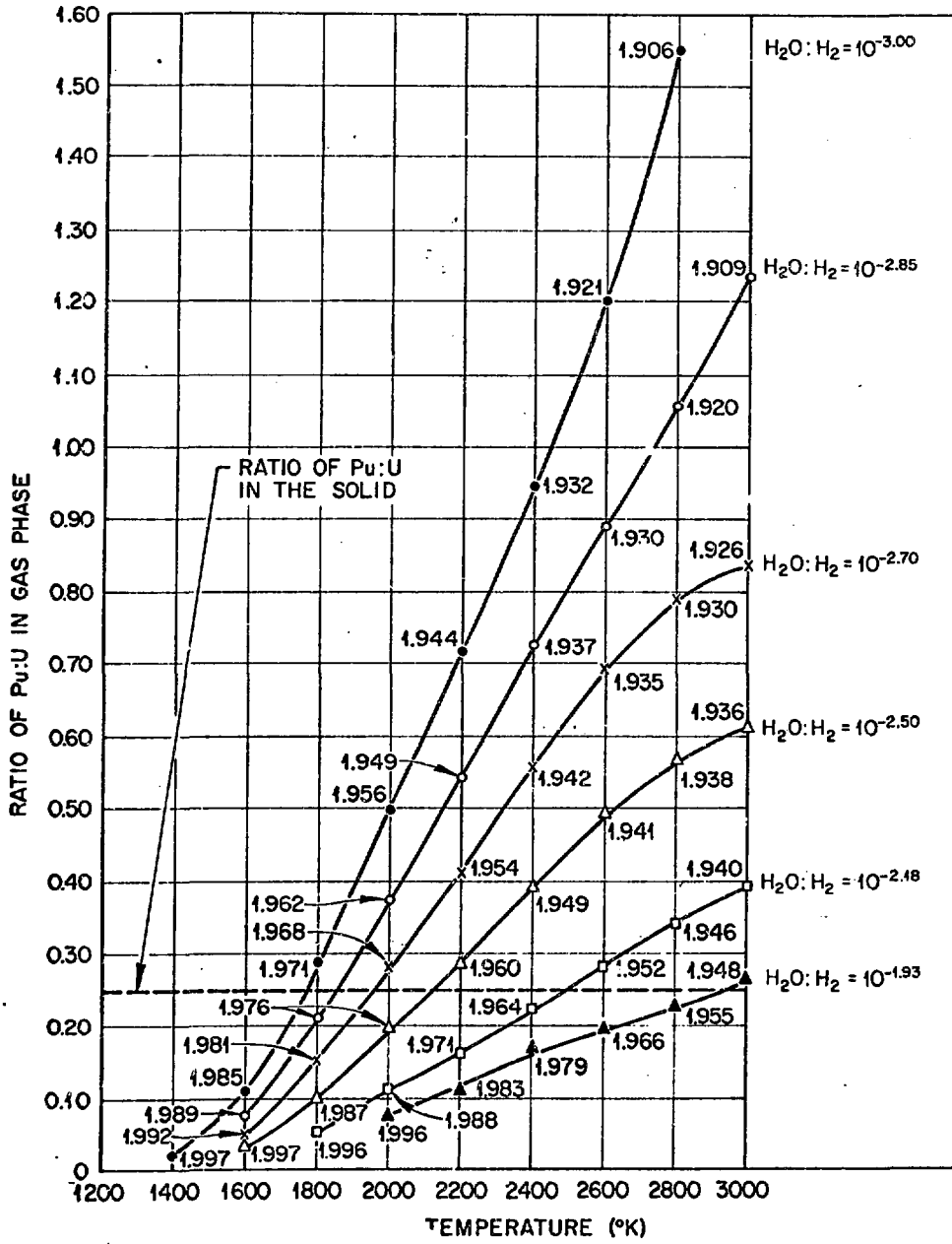


Fig. 8

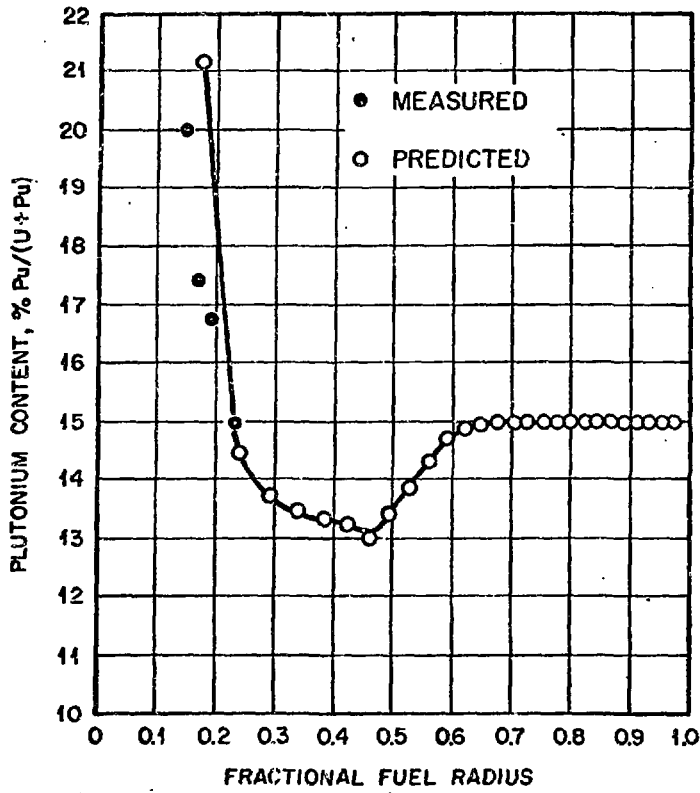
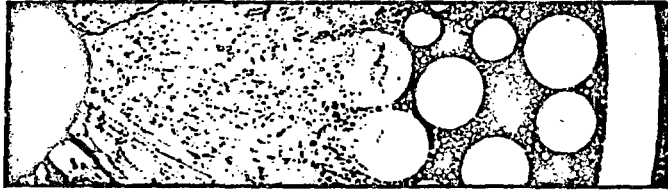


Fig. 9

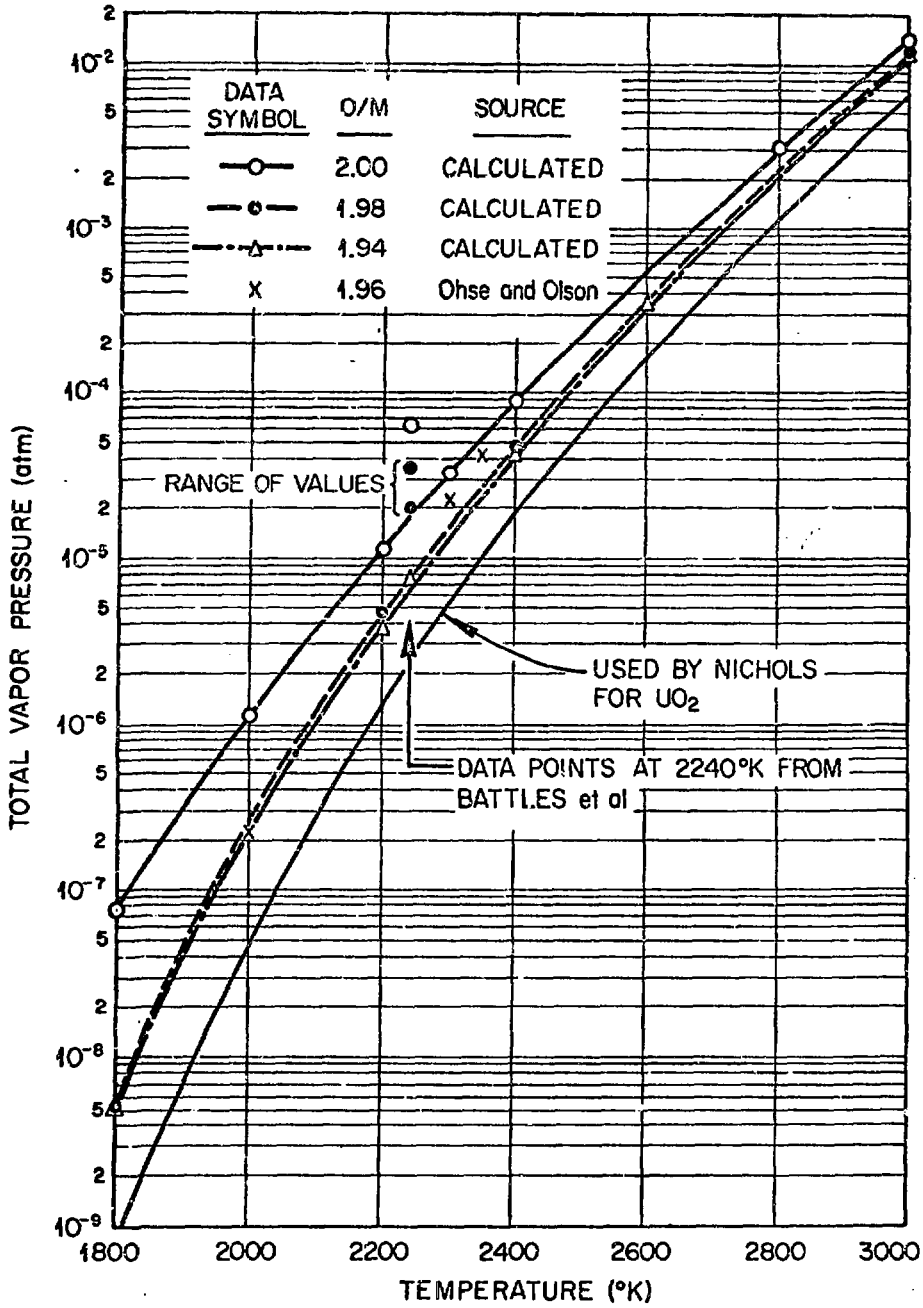


Fig. 10